MULTI-WAVELENGTH OBSERVATIONS OF CMES AND ASSOCIATED PHENOMENA

Report of Working Group F

M. PICK[1,*], T. G. FORBES[2], G. MANN[3], H. V. CANE[4], J. CHEN[5], A. CIARAVELLA[6], H. CREMADES[7], R. A. HOWARD[8], H. S. HUDSON[9], A. KLASSEN[3], K. L. KLEIN[1], M. A. LEE[2], J. A. LINKER[10], D. MAIA[11], Z. MIKIC[10], J. C. RAYMOND[12], M. J. REINER[13], G. M. SIMNETT[14], N. SRIVASTAVA[15], D. TRIPATHI[7], R. VAINIO[16], A. VOURLIDAS[8], J. ZHANG[17], T. H. ZURBUCHEN[18], N. R. SHEELEY[8] and C. MARQUÉ[8]

[1]*LESIA, UMR 8109 CNRS, Observatoire de Paris, Meudon, France*
[2]*Institute for the Study of Earth, Oceans, and Space, Univ. of New Hampshire, Durham, NH, USA*
[3]*Astrophysikalisches Institut Potsdam, Potsdam, Germany*
[4]*Laboratory for High Energy Astrophysics, NASA/GSFC, Greenbelt, MD, USA; and Bruny Island Radio Spectrometer, Tasmania, Australia*
[5]*Plasma Physics Division, US Naval Research Laboratory, Washington, DC, USA*
[6]*INAF Osservatorio Astronomico di Palermo, Palermo, Italy*
[7]*Max-Planck-Institut für Sonnenforschung, Katlenburg-Lindau, Germany*
[8]*E. O. Hulburt Center for Space Research, Naval Research Laboratory, Washington, DC, USA*
[9]*Space Sciences Laboratory, University of California, Berkeley, CA, USA*
[10]*Science Applications International Corporation, San Diego, CA, USA*
[11]*CICGE, Observatório Astronómico Prof. Manuel de Barros, Faculdade de Ciências da Universidade do Porto, Vila Nova de Gaia, Portugal*
[12] *Harvard-Smithsonian Center for Astrophysics, Cambridge, MA, USA*
[13]*Center for Solar Physics and Space Weather, Catholic University of America, Washington, DC; and NASA Goddard Space Flight Center, Greenbelt, MD, USA*
[14]*School of Physics and Space Research, University of Birmingham, U.K.*
[15]*Udaipur Solar Observatory, Physical Research Laboratory, Udaipur, India*
[16]*Department of Physical Sciences, University of Helsinki, Helsinki, Finland*
[17]*Center for Earth Observing and Space Research, Institute for Computational Sciences, George Mason University, Fairfax, VA, USA*
[18]*Dept. of Atmospheric, Oceanic, and Space Sciences, Univ. of Michigan, Ann Arbor, MI, USA*
*(*Author for correspondence: E-mail: monique.pick@obspm.fr)*

(Received 2 December 2004; Accepted in final form 6 June 2006)

Abstract. This chapter reviews how our knowledge of CMEs and CME-associated phenomena has been improved, since the launch of the SOHO mission, thanks to multi-wavelength analysis. The combination of data obtained from space-based experiments and ground based instruments allows us to follow the space-time development of an event from the bottom of the corona to large distances in the interplanetary medium. Since CMEs originate in the low solar corona, understanding the physical processes that generate them is strongly dependant on coordinated multi-wavelength observations. CMEs display a large diversity in morphology and kinematic properties, but there is presently no statistical evidence that those properties may serve to group them into different classes. When a CME takes place, the coronal magnetic field undergoes restructuring. Much of the current research

Space Science Reviews (2006) 123: 341–382
DOI: 10.1007/s11214-006-9021-1

is focused on understanding how the corona sustains the stresses that allow the magnetic energy to build up and how, later on, this magnetic energy is released during eruptive flares and CMEs. Multi-wavelength observations have confirmed that reconnection plays a key role during the development of CMEs. Frequently, CMEs display a rather simple shape, exhibiting a well known three-part structure (bright leading edge, dark cavity and bright knot). These types of events have led to the proposal of the "standard model" of the development of a CME, a model which predicts the formation of current sheets. A few recent coronal observations provide some evidence for such sheets. Other more complex events correspond to multiple eruptions taking place on a time scale much shorter than the cadence of coronagraph instruments. They are often associated with large-scale dimming and coronal waves. The exact nature of these waves and the physical link between these different manifestations are not yet elucidated. We also discuss what kind of shocks are produced during a flare or a CME. Several questions remain unanswered. What is the nature of the shocks in the corona (blast-wave or piston-driven?) How they are related to Moreton waves seen in Hα? How they are related to interplanetary shocks? The last section discusses the origin of energetic electrons detected in the corona and in the interplanetary medium. "Complex type III-like events," which are detected at hectometric wavelengths, high in the corona, and are associated with CMEs, appear to originate from electrons that have been accelerated lower in the corona and not at the bow shock of CMEs. Similarly, impulsive energetic electrons observed in the interplanetary medium are not the exclusive result of electron acceleration at the bow shocks of CMEs; rather they have a coronal origin.

1. Introduction

M. PICK, T. FORBES, G. MANN

Since their discovery in 1971 (Tousey, 1973), coronal mass ejections (CMEs) have been observed and analyzed by numerous ground-based and spaceborne white-light coronagraphs. The Solar Maximum Mission (SMM) in particular, enabled detailed analyses of the basic properties of CMEs to be made for nearly a complete solar cycle. The nearly continuous solar coverage provided by the very sensitive SOHO/LASCO coronagraph, which represents a very significant advancement over all previous spaceborne coronagraphs, has greatly benefited from the comprehensive solar and heliospheric data made available by experiments on a vast array of Earth-orbiting and heliospheric spacecrafts (TRACE, ACE, GOES, Yohkoh, Ulysses, Voyager, Wind) as well as by ground-based instruments (magnetographs, Hα telescopes, radio imaging and spectral instruments, and coronagraphs). Comparison of the CME observations from SOHO instruments with complementary observations in the low corona have, for the first time, made it possible to continuously follow the detailed progression of CME phenomena from the low corona to the interplanetary medium. In this report, we have selected topics in which joint coronal observations obtained using complementary observational and analysis techniques have been crucial in shaping our current understanding of CMEs and CME-associated phenomena.

CMEs are complex, large-scale magnetic structures, expelled from the sun and made visible by their enhanced plasma density. The full dynamical evolution of a CME includes three phases: (1) an initiation phase, (2) an acceleration phase, and

(3) a propagation phase. The period of continuous acceleration is quite variable: it can last from a few minutes to several hours and the CME, which becomes fully developed during this period, can travel a distance from a fraction of a solar radius to several solar radii. Although CMEs are a complex and varied phenomena, can we identify distinct classes of CMEs, based on their dynamic behavior and/or magnetic structure? Are the disparities observed between different CMEs due to the complexities of the coronal structures?

CMEs are often associated with eruptive prominences or disappearing filaments on the solar disk. In these cases, the CMEs most often contain three distinct regions: a bright front that surrounds a dark cavity and an inner bright core. While it is sometimes assumed that the leading edge is a compressive wave front, there is little evidence for that except for a few shock wave observations. In many cases the "leading edge" may just be coronal plasma piled up in front of the CME as it moves outward. The interior structure of CMEs has often been identified as a flux rope (see Schwenn *et al.*, 2006, this volume). However modeling of the CME formation is a controversial topic: is the flux rope the cause or a consequence of the eruption? The so-called "standard model" (see Figure 6 of Hudson *et al.*, 2006), this volume) predicts the formation of a current sheet. Do recent coronal observations provide evidence for the formation of such a current sheet?

CMEs frequently have a much more complex structure. They involve multiple magnetic flux systems and neutral lines. They are often associated with flares and/or on-disk manifestations, which have been observed in EUV as large-scale dimmings and coronal waves, and in soft X-rays as large scale and trans-equatorial loops. The exact nature of the coronal waves is unknown: are these waves different from the well-known Moreton waves identified as the chromospheric trace of a blast wave? We note that while Moreton waves are systematically associated with type II radio bursts, EUV coronal waves may have no association. What is the physical link between EUV waves and CMEs? Do they represent restructuring of the corona?

One common view, which emerged in the 1980s, is that CMEs are not directly caused by flares and that flares are not necessarily the dominant energetic phenomena in the corona. They are now recognized as two different aspects of a common magnetic energy instability and release, but the physics behind the association remains poorly understood: Can the currently available observations provide an unambiguous description of their respective temporal and spatial evolution and their respective source of energy release? For example, radio imaging observations provide information on the location of regions of magnetic interaction in the corona. These regions are the sites of electron acceleration that generate various radio signatures often observed in the decimeter-meter (dm-m) wavelength domain; electron beams escaping from these regions produce type III radio bursts, which trace the open magnetic field and coronal loop-like shapes as trans-equatorial loops (J and U bursts). The high cadence of radio observations may allow us to follow the progression and development of CMEs in the corona.

The large-scale restructuring of the corona observed during the development of CMEs suggests that for a given event, different populations of energetic electrons (and possibly protons) may be accelerated by different physical mechanisms at different times and from different coronal sites. Do recent observations contradict the commonly-held view that CME bow shocks are the exclusive source generating large SEP events, observed in the interplanetary medium?

The existence of coronal shocks was recognized early from the interpretation of radio type II bursts. Two types of shocks have been considered to produce the type II bursts: Coronal shocks which generate metric type II bursts, currently attributed to blast waves originating in the flare-region; and CME-driven shocks, which produce hectometric-kilometric type II bursts during their propagation in the interplanetary medium. As coronal and interplanetary type II bursts can be produced during the same event, there is a continuing controversy on the relationship between type II bursts (coronal shocks), flares, and CMEs. At what altitude can CME-driven shocks form? Can we detect shocks by remote techniques other than radio observations such as EUV, X-ray and white light?

A summary of the questions and conclusions by this working group is presented in the following sections.

2. Coordinated Multi-Wavelength Signatures of CME Development

R. A. HOWARD, N. SHEELEY, J. ZHANG, N. SRIVASTAVA, G. SIMNETT, J. CHEN, M. PICK, C. MARQUÉ

To understand CME phenomena, it is essential to utilize observations in addition to those from the white-light coronagraph. While attempts have been made to develop a proxy for the coronagraph, the clear identification of when and where a CME has occurred is still best made with the coronagraph. However, the coronagraph measures only the density properties of the CMEs. The combination of all the space-based experiments currently available and the extensive network of ground based instruments present an unprecedented opportunity to characterize CME phenomena all the way from the surface of the Sun out to interplanetary space. Furthermore, the ground-based telescopes are able to acquire data at a much higher cadence than the space-based telescopes. These multi-wavelength observations can tell us: (1) What is the sequence of events below the coronagraph occulting disk? (2) What occurs first and in what time order? (3) What structures are involved in the energy release?

2.1. DIVERSITY OF CMES

Coronal mass ejections display diversity in morphology and kinematic properties. Frequently, large and bright CMEs display a three-part structure, namely the bright

frontal or the leading edge, followed by a dark cavity and a bright knot often associated with prominence material. Well-organized helical structures within CMEs have often been observed by LASCO (Dere *et al.*, 1999), CDS (Pike and Mason, 2002), and UVCS (Antonucci *et al.*, 1997; Ciaravella *et al.*, 2000). The classification of a CME in terms of its structure and morphology was first done using SOLWIND white-light observations (Howard *et al.*, 1985). These structural classes included loop, curved front, halo, spike, double spike, streamer blowouts and, as the names suggest, are based on the shape of the CMEs. They termed another class of CMEs as "complex," which were irregular in shape and did not fit in the other sub-classes. It is now becoming clear that many events are in fact multiple eruptions closely spaced in time and projected on the plane of the sky.

Another type of classification scheme based on signatures of field line disconnection was discussed by Webb and Cliver (1995). They found that about 10 % of all CMEs had disconnection features, defined as transient large-scale, concave-outward bright regions usually following the CME leading edge. Such disconnected structures were previously observed in SMM images as U-shaped features by McComas *et al.* (1991). The disconnected features of CMEs have been found to retain their shapes out to a distance of 28 solar radii in LASCO images, as shown by Simnett *et al.* (1997), while other observations show that some CMEs show little evidence of disconnection (Chen *et al.*, 1997, 2000). Although a CME often refers to a large-scale phenomenon, narrow CMEs have been reported (Gilbert *et al.*, 2001; Wang and Sheeley, 2002; Yashiro *et al.*, 2003; Dobrzycka *et al.*, 2003) as have very faint CMEs (Lyons and Simnett, 2001). At the smaller end of the scale, Sheeley *et al.* (1997) have studied tiny eruptions which they called "blobs". Because coronagraph observations yield two-dimensional (2-D) projections of intrinsically three-dimensional (3-D) structures, the true 3-D morphology of observed CMEs is not yet definitely established. Nevertheless, all existing 3-D models indicate that after the eruption, CMEs can be understood as expanding flux ropes (Chen *et al.*, 1997; Wu *et al.*, 1999; Amari *et al.*, 1999; Krall *et al.*, 2001; Tokman and Bellan, 2002).

A classification scheme based on kinematic properties was first done by MacQueen and Fisher (1983). Based on inner coronal observations (i.e. from 1.2 to $2.4 R_\odot$ by the ground-based MK3 coronagraph), they found that large flare-associated events exhibit high speeds (>700 km s^{-1}) and little acceleration (0.3 m s^{-2}) with height while the eruptive-filament-associated events start with low speeds of 10–20 km s^{-1} and exhibit accelerations from 0–50 m s^{-2}. Based on outer corona observations (from 2.0 to $30.0 R_\odot$ by the LASCO C2/C3 coronagraphs), Sheeley *et al.* (1999) also suggested the existence of two classes of events: the so-called impulsive and gradual CMEs. Impulsive CMEs show constant speed typically greater than 750 km s^{-1}, implying a short but strong acceleration in the inner corona. Gradual CMEs display a persistent and weak acceleration with their leading edges accelerating gradually to speeds in the range 400–600 km s^{-1} before leaving the LASCO field of view. Based on combined LASCO C1/C2/C3 observations, Srivastava *et al.*

(1999) presented a number of gradual or balloon-type events that start off with very low speeds (<100 km s^{-1}) below 3 solar radii and attain a maximum value of acceleration ranging between 5–25 m s^{-2}, which occurs between 3–6 $R_{\odot}$. These observations indicated that gradual-type events generally drift away in the slow solar wind. A similar classification scheme was proposed by Andrews and Howard (2001) but with different names: Type C (Constant speed) events versus Type A (Acceleration) events. Based on a large number of LASCO CME events, St. Cyr *et al.* (1999) and Moon *et al.* (2002) made a statistical study about the differences between flare-associated CMEs and eruptive-filament-associated CMEs and found a tendency for flare-associated CMEs to be faster.

Nevertheless, there is not yet convincing statistical evidence to suggest the existence of two distinct classes of events. In terms of speed, it has been consistently shown that there is a continuous distribution of speed from tens of km s^{-1} to about 2500 km s^{-1} with a single peak at about 300–400 km s^{-1} (Howard *et al.*, 1985; Hundhausen *et al.*, 1994; St. Cyr *et al.*, 2000; Yashiro *et al.*, 2003). However, the peak is in part due to the selection criteria used to define a CME in these studies, which favor the bright, large-scale events. In terms of acceleration, (Zhang *et al.*, 2004) demonstrated that the magnitude of the acceleration in the inner corona can vary by three orders of magnitude, i.e., from a few m s^{-2} to several thousand m s^{-2}. Further, the duration of the acceleration can vary by the same magnitude, i.e., from a few minutes to several hours. The existing data do not support a bimodal distribution of CME acceleration.

Despite the failure to identify objective signatures that place CMEs in separate statistical classes, we know that all CMEs are not alike. In fact, in studying different kinds of CMEs we have been able to gain insight into the physical mechanisms.

In the next several sections, we give an overview of different types of CMEs and some physical insights that have been gained by the multi-spectral approach.

2.2. Small Exploding Flare Events with Reconnection

The initiation of a CME in EUV was first detected by EIT (Dere *et al.*, 1997). In this paper a small, compact bubble is seen to form and propagate outward. It was seen in the LASCO/C1 Fe XIV channel and then subsequently in the LASCO/C2 as a small enhancement along a pre-existing streamer. Innes *et al.* (1999) used several different telescopes to investigate the relationship between a CME and an X2 flare (see Figure 1). Innes *et al.* compared SOHO/CDS EUV spectrometer data, GOES X-ray flux, Yohkoh/SXT images, SOHO/EIT Fe XII images, Meudon Hα filtergraph images, Pic du Midi Hα coronagraph images and finally the LASCO/C1 Fe XIV, C2 and C3 images. In their interpretation, a filament started to rise, before the flare, forcing anti-parallel magnetic fields to reconnect and the flaring to start. A small CME started about 20 minutes after the flare and filament eruption and in between two X-ray jets. Innes *et al.* suggested that reconnection at the site of one of

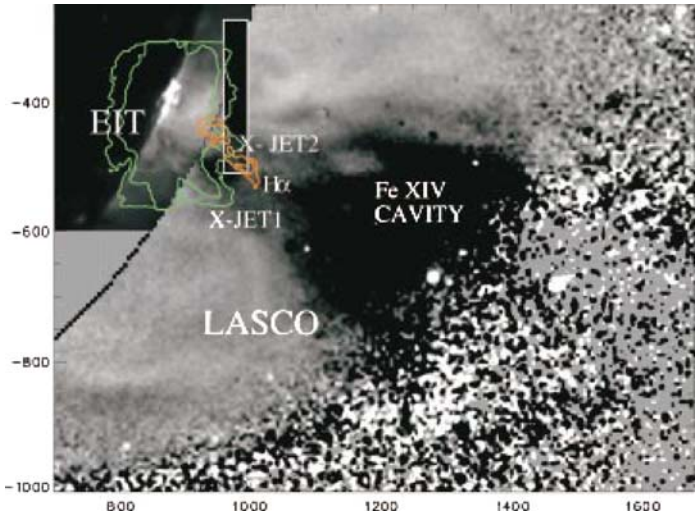

Figure 1. April 9, 1997 event. Spatial relationship between a CME and an X2 flare, as revealed by several telescopes. Shown are LASCO C1 5303 Å difference images ($>1R_{\odot}$) taken before and after the flare, as well as soft X-ray contours (shown in green), Hα coronagraph contours (red) and an EIT 195 Å image ($<1.1R_{\odot}$) taken after the flare. The position of the CDS raster is outlined in white (Innes *et al.*, 1999).

the jets (at one footpoint) triggered reconnection at the other footpoint (producing the second jet).

Complimentary observations of these explosive, flare-related CMEs have been obtained with the TRACE, Yohkoh/SXT and GOES12/SXI instruments (McKenzie and Hudson, 1999; Gallagher *et al.*, 2002; Innes *et al.*, 2003; Asai *et al.*, 2004). These observations have revealed inward motions in the hot (15 MK) plasma cloud that forms in the region evacuated by the CME. In a time of about 30–40 min, the elements of the cloud move inward and cool from ∼15 MK to <1 MK, becoming visible as the familiar structures we call flare loops. One by one, the individual loops in the lower-temperature emission lines disappear and are replaced by higher loops moving in from above. This accounts for the rising locus that is typically observed and often seen as radio continuum. Kerdraon *et al.* (1983) observed stationary type IV radio emission in the position of the legs of a CME, presumably in the region of post-eruptive restructuring of the corona where the flare loops were being formed. Kahler and Hundhausen (1992) suggested these type IV bursts could be associated with newly formed streamers.

Comparing SOHO/LASCO and EIT images of narrow, high speed CMEs (called jets) during the rising phase of the sunspot cycle, Wang *et al.* (1998) found that narrow (∼2–4 degrees), fast (∼600–1000 km s^{-1}) white-light jets in the C2 and C3 fields of view were the extensions of EUV jets seen by EIT. These jets appeared when small bipoles emerged in polar coronal holes. Wang *et al.* (1998) suggested

that the jets originated when the closed field of the newly emerged flux reconnected with the open fields of the polar holes (interchange reconnection), thereby allowing material to slip outward along the open field lines. In a second study, Wang and Sheeley (2002) made a similar comparison near sunspot maximum. They found that in this epoch, when polar fields were weak and the polar holes were gone, the jets came from places where newly emerging flux penetrated coronal holes well outside the Sun's polar caps. UVCS and EIT observations of polar jets show relatively low temperatures, consistent with heating at the base of the jets (Dobrzycka *et al.*, 2002).

In a separate study, Kahler *et al.* (2001) noted that a 960 km s^{-1} jet was associated with an impulsive solar energetic particle event at the Wind spacecraft. They suggested that such jet-like CMEs might correspond to the SXT X-ray jets and type III radio bursts observed previously by Raulin *et al.* (1996), and that these type III burst electrons may provide information about the magnetic topology of CMEs that are accompanied by impulsive flares. The Nançay Radioheliograph (NRH) images for this event revealed a series of type III-like sources moving outward at the same position angle as the C2 LASCO feature (Pick *et al.*, 2003).

2.3. CMEs and Prominence Eruptions

Prominence eruptions (EPs) frequently accompany CMEs. Gilbert *et al.* (2000) and Gopalswamy *et al.* (2003) found that more than 72% of Hα erupting prominences are associated with CMEs. Gopalswamy *et al.* also noted that the latitude distributions of EPs and CMEs both peaked at the equator around sunspot minimum.

An example of a class of CME events that is not usually associated with impulsive disk phenomena was discussed by Srivastava *et al.* (2000). For this event (displayed in Figure 2), they combined Hα images from Helio-Research (courtesy of Sara Martin), 17 GHz images from the Nobeyama Radioheliograph, LASCO/C1 Fe XIV/Fe X images, and LASCO/C2 and C3 white-light images. They found that features in the images moved very gradually upward ($<$50 km s^{-1}), with the prominence activating and moving outward, for many hours ($\sim$18) before the second phase started. At that time, the CME/prominence system accelerated quickly to over 500 km s^{-1} before decelerating down to the slower solar wind speed when it left the field of view of LASCO/C3. The minimum value of the acceleration corresponds to the slowly moving structures identified by Sheeley *et al.* (1997). They further noted that there is no observational evidence for magnetic reconnection or impulsive energy release associated with this CME. Howard *et al.* (1986) showed that this class of events did not exhibit a solar-cycle dependence, indicating that the cause of such eruptions occurs at a constant rate throughout the cycle. Differential rotation and the subsequent shearing of coronal fields has been explored as possible CME initiation mechanism (e.g. Linker and Mikic, 1995; Forbes *et al.*, 2006).

This kind of event usually generates the three-part structure. In the dm-dam wavelength domain, thermal emission is detected in association with the filament

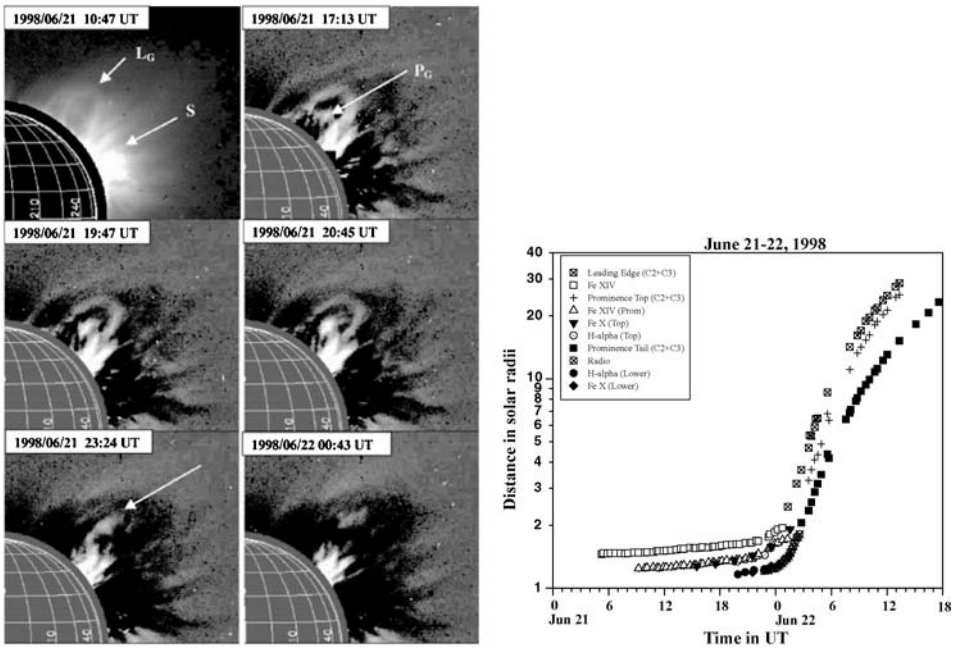

Figure 2. June 21–22, 1998 event. *Left*: Time-lapse images taken by LASCO-C1 coronagraph in Fe XIV emission line. The field of view is 1.1–3 $R_{\odot}$. All the images shown here have been subtracted from a reference image taken before the occurrence of the CME, except the image taken at 10:47 UT. The 10:47 UT frame is an on-line image with a nearby continuum and shows the bright streamer adjacent to the CME. *Right*: Plot of height (on a log scale) against time for different features of the CME: the leading edge, the prominence top, and prominence tail. These features were tracked using several instruments at different wavelengths (Srivastava *et al.*, 2000).

cavity; thermal emission is weak and often masked by the presence of non-thermal radio burst emission. Metric observations are, however, able in favorable cases to probe the filament cavity and make the link with the CME cavity (Marqué *et al.*, 2002). CME thermal detection in radio has a great potential interest because of the ability to determine mass and density of a CME (Sheridan *et al.*, 1978; Gopalswamy and Kundu, 1992). Despite these earlier attempts, a clear distinction between thermal and non-thermal contributions remains difficult to establish.

2.4. LARGE-SCALE CMES

The development in the low corona of large flare/CME events is often fast and is accompanied by an opening of the magnetic field over a large region. Large scale dimming observed in EUV and soft X-rays and disappearing transequatorial loops are signatures of the opening of the magnetic field. Li *et al.* (2001) have developed a technique to show the field lines that have opened up as a result of the CME event.

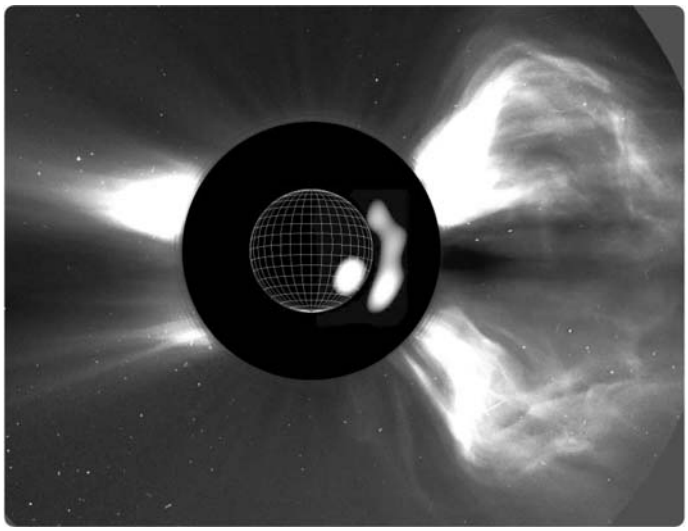

Figure 3. November 6, 1997 event. Composite image of a LASCO/C2 CME image with a radio NRH image at 164 MHz showing that there is a close correspondence between the extent in latitude of the CME seen by LASCO- C2 and the sites of radio emission (adapted from Maia *et al.*, 1999).

Coronagraphs observe limb CMEs better than halo CMEs. For the large, fast CME that occurred on the west limb on 6 November 1997 (see Figure 3), Maia *et al.* (1999) related the radio observations to the optical observations seen all the way down to $1.1 R_{\odot}$ by the LASCO/C1, which observed the CME in Fe XIV and Fe X emission. This CME expanded laterally from a relatively small angular size, in the vicinity of the flare site and reached its full size in the low corona within 5 minutes. A close association between the location of radio emission and the white-light CME structure was seen. It is interesting to compare these observations with those of an on-disk event because the two perspectives give us a more complete picture. Pojholainen *et al.* (2001) for the on-disk event on 2 May 1998 linked, both spatially and temporally, a propagating disturbance to the successive radio source components of a coronal type II burst and to an Hα Moreton wave propagating away from the flare region. Khan and Hudson (2000) suggested that, in the case of the 2 May 1998 event, the wave also causes the destabilization of the interconnecting loop structure seen in X-rays. Both these limb and on-disk events showed a similar spreading of radio sources. The full expansion of these events took place in the low corona within 5–15 minutes.

A well-studied event is the Bastille-day event, which occurred on 14 July 2000, and for which a number of papers have been published in a single volume in Solar Physics (special issue, 204/1–2, 2001). This event illustrates many points that will be discussed in the following sections. During July, the active region 9077 produced intense activity, which culminated in an X7.5 flare and a major CME

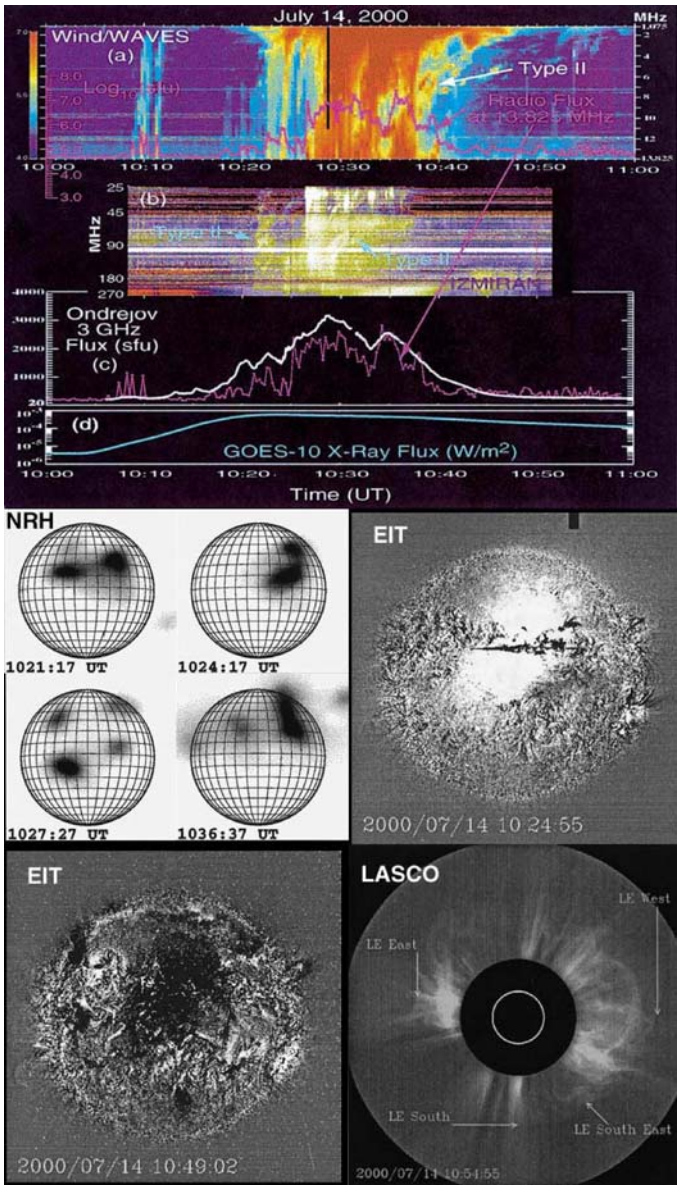

Figure 4. July 14, 2000 event. *Upper panel*:(a) Dynamic spectra of the Wind/WAVES radio emission; (b) IZMIRAN dynamic spectrum of the metric radio emissions; (c) Intensity versus time of the Ondrejov decimeter data of 3 GHz and of the flux measured by Wind at 13.825 MHz ; (d) GOES X-ray flux. *Middle and lower panels*: Images from the NRH at 164 MHz, EIT at 195 Å and LASCO-C2 illustrating the development of the CME above the solar disk and above the solar limb (references in Solar Physics, special issue, 204-1-2, 2001).

on July 14. Accompanying this activity were radio emission, energetic particles, interplanetary shocks, and interplanetary magnetic clouds. Figure 4 displays a series of observations obtained at different wavelengths. The LASCO images show that besides the loop-like CME on the west limb, there are several bright discrete features all around the Sun. Most of the solar disk was affected by the CME development. The EIT observations show a brightening of a large area of the corona followed by a dimming over roughly the same region, suggesting that the bright material had been ejected. The development of the radio event is reminiscent of that of the May 02 1998 event: In less than 15 minutes, large-scale loops spanned the entire disk, apparently in association with spectral drift type II emission. The type II emission was accompanied by very intense, complex, long duration type-III like radio emission over a very large spectral range (Figure 4; upper panel a, b, c). The close similarity in the 3 GHz and 13.82 MHz profiles of the radio emission indicates that radio emission detected by WAVES at kilometric wavelengths was produced by electrons accelerated in the coronal regions seen in the NRH images (see Section 6.3).

2.5. EIT Waves, Coronal Dimming and CMEs

EIT waves are large disturbances that travel across the disk of the Sun (Moses *et al.*, 1997; Thompson *et al.*, 1998). An unambiguous correlation between EIT waves and CMEs was found by Biesecker *et al.* (2002). The EIT-wave/shock association is considered in more detail in Section 5. An important signature of on-disk CMEs (i.e. halos) are the soft X-ray dimmings (Sterling and Hudson, 1997) observed in the Yohkoh/SXT. The dimming is ascribed to a mass deficit, $\sim 10^{14}$ g, which is consistent with the amount of material that erupts. In contrast to the EIT wave or Moreton wave, the X-ray dimming appears suddenly like transient coronal holes on the Sun's disk. Additional discussion of EIT waves can be found in Section 5.2.

3. Magnetic Reconnection

T. G. Forbes, H. S. Hudson

3.1. Theoretical Framework

The concept of magnetic reconnection arises from the idea that the topology of the magnetic field plays an important role in the forces acting on the plasma (Biskamp, 2000; Priest and Forbes, 2000). In a non-conducting fluid, or vacuum, the topology of the field has little theoretical value, and the magnetic field can be represented exactly in terms of a potential. Within the framework of MHD theory as applied to a magnetized plasma, however, dynamical effects do arise. Currents can flow within the plasma, stressing the field away from the relaxed state. Relaxation nearer to

this unstressed state, if on a short time scale, is equivalent to the breakdown of the adiabatic invariants of the particle motion (e.g., (Northrop, 1966). This reflects the physical definition of a magnetic field line in terms of particle motion. The concept of reconnection inherently requires a breakdown of the ideal MHD approximation.

When a CME takes place, the coronal field undergoes a radical restructuring on a time scale short relative to the resistive time scale of the medium in what is, for the most part, a low-β plasma. Prior to the onset of the CME, the coronal field has gradually accumulated stresses related to forces acting below the photosphere. In some models, the coronal magnetic structure is presumed to be organized into topologically distinct cells divided by surfaces termed separatrices. A flare and/or CME corresponds to a transfer of magnetic flux between the cells. In the case of a CME the restructuring implies the opening of some magnetic flux, in the sense that previously closed loops become greatly extended. The main theoretical problem of flares and CMEs is to explain not only why energy is released, but also why the corona is able to sustain the stresses that allow an energy build-up (see in this volume (Mikić and Lee, 2006; Forbes *et al.*, 2006).

3.2. Relevant Observations

At present we have many solar signatures, in flares and in CME counterparts in the low corona, consistent with the general idea of magnetic reconnection. This list below could be extended in the near future, although necessarily only via indirect remote-sensing techniques. It is striking that reconnection signatures are relatively rare in the coronagraph field of view so that if reconnection plays a major role in CMEs it is likely to do so at lower altitudes. It is not yet possible to say whether magnetic reconnection plays an important role in the onset of an event. In particular we do not know if reconnection triggers a flare or simply results from a flare. Even more fundamentally, since MHD physics cannot self-consistently describe the all-important particle populations, we know that additional physics describing kinetic effects is important. At the present time very little theoretical development has occurred to incorporate such kinetic effects within the larger framework of the MHD flows.

3.2.1. *Ribbon Morphology*

The existence and motions of Hα flare ribbons strongly motivated the basic idea of the coronal reconnection models. The fact that the outer edge of the ribbon propagates by the lighting up of the existing chromospheric fibril structure is a strong indicator that the flare energy source is continually moving onto new field lines as required by reconnection. Furthermore, the existence of a one to two arcsecond wide band of strongly red shifted Hα emission along the outer edges of the ribbons (Svestka *et al.*, 1980) also supports the reconnection model. The outer edges of the ribbons are expected to be strongly heated by conduction electrons or energetic particles propagating along field lines mapping directly to the reconnection site.

The heating produces a downward flow of cool plasma in the chromosphere and an upward flow of heated plasma in the corona (Doschek *et al.*, 1983). Recent EUV spectroscopic imaging from SOHO/CDS has provided strong evidence that the corresponding upflow of heated plasma does exist at the outer edges as required (Czaykowska *et al.*, 1999).

3.2.2. *Hard X-ray Timing*

The hard X-ray footpoint sources exhibit strongly correlated fluctuations, consistent with the acceleration of electrons high in the corona. This result, originally due to Yohkoh/HXT, has now been extended by the finding that the footpoint spectra also match (Krucker and Lin, 2002). Coronal particle acceleration suggests coronal energy release, since we know that the particles (>10 keV electrons) contain a large fraction of the total energy.

3.2.3. *Cusp-Shaped Structure*

Soft X-ray images, such as those from Yohkoh/SXT, often show cusp-shaped features, especially in the late phase of a CME-related solar flare. The cusp may have an elevated temperature (Tsuneta *et al.*, 1992) and thus this morphology points to an energy source in the solar corona – *ergo*, large-scale reconnection along the lines of many models.

3.2.4. *"Above-the-Loop-Top" Source*

The discovery by Masuda *et al.* (1994) of an *above-the-loop-top* hard X-ray source suggested the reconnection geometry more directly. The interpretation considers a fast reconnection outflow jet from a reconnection point high in the corona, which then impinges on closed field lines and particle acceleration by shock waves or turbulence resulting from this.

3.2.5. *Supra-Arcade and LASCO Downflows*

Soft X-ray and EUV observations frequently show a fan of spikes extending above the loop system of a flare arcade. McKenzie and Hudson (1999) found dark features moving downward through this fan. They refer to these features as "voids" and interpret them as three-dimensional equivalents of the magnetic islands produced by the tearing mode. Voids occur during both the impulsive and gradual phases of flare evolution (Innes *et al.*, 2003; Asai *et al.*, 2004). In addition to the rapid motion of the voids, a general downward flow pattern exists in the arcade structure even as its upper edge increases in height (Sheeley *et al.*, 2004).

Downflows of two types have been directly seen in LASCO white-light images (Sheeley *et al.*, 2004) describe features similar to the supra-arcade downflows ("tadpoles") at altitudes of 2–4 $R_{\odot}$, much later than the eruption and exhibiting smaller inflow speeds. They identify such inflows with a continuation of the reconnection process implied by the observations in the flare arcades. These are also void regions

(Sheeley and Wang, 2002). The other (much less frequent) type of outer coronal downflow has both upflows and downflows, and more nearly resembles the classical picture of reconnection in the sense of disconnection (Sheeley and Wang, 2002; Simnett, 2004).

3.2.6. *Sigmoid and Dimming*
Sterling and Hudson (1997) found a characteristic X-ray morphology to be associated with CME formation, as detected by the formation of "transient coronal holes," a form of X-ray dimming originally identified in Skylab soft X-ray images. The sigmoid, identified with a hot component aligned with a filament channel, evolves during the event into an arcade perpendicular to it. This suggests "dipolarization" responsible for energy release following reconnection.

3.2.7. *Inflow into X-line*
The cusp configuration, if it reflects continuing magnetic reconnection, implies an essentially horizontal inflow into the X-point (in two dimensions). This has been surprisingly hard to detect, perhaps because the inflowing plasma should be extremely low-density because it is on open or opening field lines; nevertheless Yokoyama *et al.* (2001) have found a clear case, combining both soft X-ray and EUV data, of a large-scale coronal cusp with strong evidence for just such an inflow.

3.2.8. *Bidirectional Type III Radio Bursts*
Type III radio bursts have a strong association with the impulsive energy release in a solar flare, and reveal the presence of beams of non-thermal electrons. Bidirectional type III bursts, as observed by Aschwanden *et al.* (1995), show that these beams appear to diverge from the intersection of magnetic structures. This technique of inferring magnetic field line reconnection from bi-directional type III bursts is analogous to the technique of inferring coronal or heliospheric field line reconnection from bi-directional electron heat fluxes in the in-situ solar wind (Crooker *et al.*, 2002; Simnett, 2004).

4. Observational Signatures of Current Sheets

A. CIARAVELLA, H. S. HUDSON

4.1. THEORETICAL FRAMEWORK

The "standard model" for the development of an eruptive flare or of a CME involves the expansion of closed coronal magnetic fields (e.g. Anzer and Pneuman, 1982). As this bubble of bipolar magnetic field moves outwards, an inflow occurs behind it, driven by external magnetic pressure. The outward flow creates elongated field lines

with appropriate orientation (opposed fields) to form a current sheet and ultimately to reconnect, and this reconnection then explains the formation of the arcade of flare loops. Coronal observations now provide some evidence for the formation of the current sheet that the standard model envisions.

4.2. Relevant Observations

4.2.1. *CME Morphology*

CMEs typically leave vertical linear features behind them; these have often been interpreted as "legs," in other words unipolar structures that represent flux tubes. Kahler and Hundhausen (1992) however pointed out that an alternative interpretation could be made that some legs were in fact current sheets. If so, this would support the basic tenet of the standard model and would explain the lack of transverse (lateral) motion expected for true legs to display as reconnection proceeded (Webb *et al.*, 2003). Early attempts towards the same end involved searches for "disconnection" events, motivated by the 2D cartoon representation of the standard model in which magnetic fields actually must disconnect from the surface of the Sun (Illing and Hundhausen, 1983). There is some evidence for concave-up features in CME images, but instead of interpreting this evidence as disconnection the more modern view is the 3D version: the concave-up features represent the bottom of a flux rope whose ends in fact remain connected to the photosphere (see Forbes *et al.*, 2006, this volume).

4.2.2. *Spectroscopy*

Because magnetic reconnection may be occurring in the current sheet and enabling energy release, the presence of a thin spike of high-temperature material beneath a retreating CME would match the expectation of the standard model. This closely describes recent spectroscopic observations by Ciaravella *et al.* (2002) and Ko *et al.* (2003), in which narrow, bright features appeared in Fe XVIII 974 Å. An illustration of the 1998 March 23 current sheet observation (Ciaravella *et al.*, 2002) is given in Figure 5, compared with an illustration of the current sheet in the Lin and Forbes (2000) model. A similar structure was observed on 2002 January 8. Figure 6 shows a composite image of EIT, MLSO-MK4[1], CDS and Fe XVIII 974 Å line intensity distribution along the UVCS slit. The high-temperature narrow feature observed by UVCS just above the post-CME loop cusp has been interpreted as the current sheet.

These current sheets refer to heights of $1.5\,R_\odot$ and exibit very similar characteristics. Both have very long duration: 20 hours in the 1998 March 23 event and about 2 days in the 2002 January 8. Their spatial width in the Fe VXIII emission is $0.1\,R_\odot$ and $0.2\,R_\odot$, respectively. Temperatures inside the current sheet are $4-6\times10^6$ K and densities in the range $10^7 - 10^8$ cm^{-3}. In both cases the analysis of the elemental

[1]The Mauna Loa Solar Observatory Mark 4 K-coronameter.

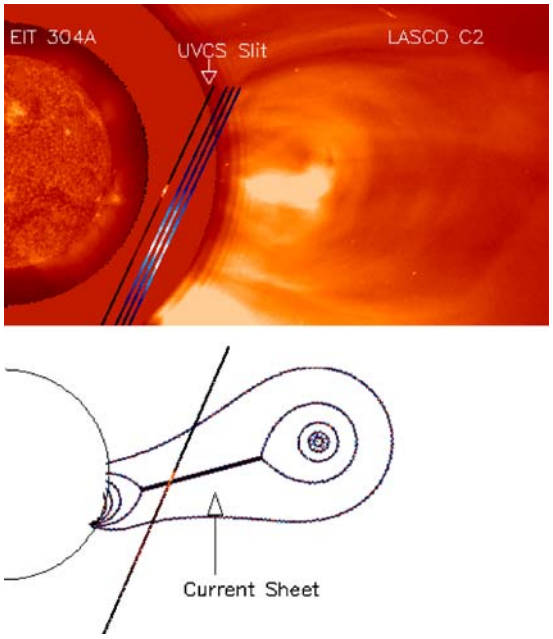

Figure 5. Composite image of EIT 304 Å (22:24 UT), LASCO C2 (12:33 UT) and line intensity distribution along the UVCS slit (16:56 UT) taken on March 23, 1998. The arrow indicates the true position of the slit and the intensity distribution shown is from the Fe XVIII 974 Å line. Three other slits are plotted for comparison and show (from left to right) the line intensity distribution of Si XII 499 Å, OVI 1032 Å, and Lyβ. The UVCS data used in this figure were taken with the slit pointed at $1.45R_{\odot}$ and position angle $PA = 245^{\circ}$. The position of the peak in the Fe XVIII line is $PA = 257^{\circ}$ and height $1.55R_{\odot}$. The different times were chosen to combine the data into a single image. At the time of the observation, the LASCO CME was much larger, but similar in shape. The flux-rope CME and the associated current sheet as predicted by the Lin and Forbes (2000) model are drawn below the composite image. Superimposed is the line intensity distribution of Fe XVIII along the slit (Ciaravella *et al.*, 2002).

abundances shows a large FIP effect[2] in which the coronal iron abundance in the 1998 March 23 current sheet, is enhanced by a factor of 7 relative to its photospheric value. The strong FIP effect in the sheets provides evidence that plasma flowing inside is from coronal origin (Ciaravella *et al.*, 2002; Ko *et al.*, 2003). Also, in the 2002 January 8 event, blobs are seen flowing along the current sheet; these were interpreted as a signature of reconnection in a non-uniform plasma by Ko *et al.* (2003).

The Lin and Forbes (2000) model provides a description of the current sheet geometry, as shown in Figure 5. Reconnection along the current sheet could help the flux rope to escape outwards. The model does not predict the physical parameters of the plasma in the sheet but the general properties such as length, position and duration of the sheet, agree with the UVCS observations. The MHD simulation of

[2]Enhancement of elements with high first ionization potential.

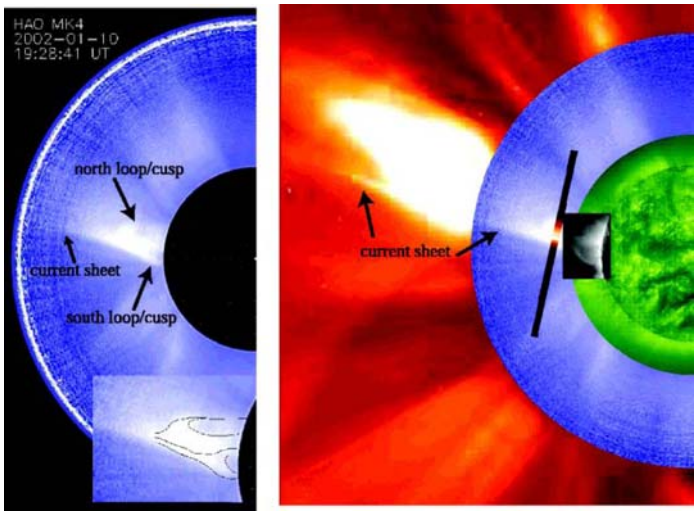

Figure 6. Left: MLSO MK4 white-light image at 19:28 UT, January 10, showing that the two loop/cusp systems still exist 2 days after the CME. The inset shows our perception of what the two loop/cusp systems might look like. *Right*: Composite image from EIT 195 Å (19:36 UT), CDS Fe XVI (small rectangle at the limb), MK4 (19:28 UT), and C2 (20:26 UT) images of January 10. Superposed on the image is the projection of the UVCS slit on the plane of the sky (the width is not to scale) showing the spatial distribution of the [Fe XVIII] 974 emission. It is clear that the high-temperature emission is along the direction of the current sheet (Ko *et al.*, 2003).

Linker *et al.* (2003) show the self-consistent formation of a similar current sheet (see Figure 3 of Forbes *et al.*, 2006, this volume).

4.2.3. *X-ray Evidence*

X-ray imaging observations of solar flares have provided evidence of a second high energy source located above the lower source. This upper source is at the right altitude to be located at the upper tip of the current sheet predicted by the standard model. Furthermore, the temperature distribution within this source is reversed to that of the lower source as would be consistent with the inverted geometry of the field at the upper tip of the current sheet (Sui and Holman, 2003). In other words, the gradient is opposite to that found at the loop top by Masuda *et al.* (1994), and together, the two sources are consistent with a hot current sheet (at small emission measure) lying between them.

Both the UV and X-ray observations add the element of plasma temperature to the streamer geometry. At the boundary between oppositely-directed magnetic fields one must have a current layer; these new data show that such a current system in CME-related structures actively heats the plasma to temperatures normally found only in solar flares. This clearly points to magnetic reconnection in the standard model as a mechanism to enable the heating to happen. The theoretical problem

(e.g., Webb *et al.*, 2003) is that current theories do not predict "how hot or dense the current sheet should be;" thus at present we have no quantitative means to link these observations to the rate of reconnection and thus to flare effects. More sophisticated models, planned for the future, may make such comparisons possible (see Mikić and Lee, 2006, this volume).

5. Coronal Shocks and Waves

M. REINER, J. C. RAYMOND, M. PICK, D. MAIA, H. S. HUDSON,
A. KLASSEN, K. L. KLEIN, G. MANN

5.1. INTRODUCTION

Coronal shock observations are important because they provide information on the characteristics and dynamics of energetic phenomena on the Sun, such as solar flares and CMEs (see in this volume Hudson *et al.*, 2006; Schwenn *et al.*, 2006). CME shocks are also involved in accelerating Solar Energetic Particles (SEPs) that are observed in interplanetary space (see in this volume (Cane and Lario, 2006; Klecker *et al.*, 2006; Mikić and Lee, 2006; Forbes *et al.*, 2006); see also (Reames, 1999). The interplanetary extension of coronal shocks, that are driven by CMEs, can significantly affect the space weather environment when they encounter Earth. Coronal shocks can presently only be observed remotely. The primary observational signature of these shocks are the radio emissions they generate as they propagate through the solar corona. These radio signatures, called metric type II bursts, have been observed from ground-based radio observatories since the early 1950s. More recently, a few coronal shocks have been observed and studied in UV, X-ray and white-light images (Vourlidas *et al.*, 2003; Raymond *et al.*, 2000).

When these shocks propagate into interplanetary space, they produce low-frequency kilometric type II radio emissions (see Forsyth *et al.*, 2006, this volume). Kilometric type II emissions are unambiguously identified with shocks that are driven by CMEs and can sometimes be observed in situ (Bale *et al.*, 1999). In-situ shock observations provide a better understanding of the nature of the radio emission mechanism, as well as the interplanetary plasma conditions and shock geometries that favor the generation of the type II radio emissions (see Forbes *et al.*, 2006, this volume). While type II radio bursts can be generated by either blast-wave or driven shocks, it is expected that only driven shocks can propagate into interplanetary space because blast-wave shocks quickly weaken with distance and are unlikely to escape the lower corona. Hence in the solar corona the problem of shock association is more complex than in interplanetary space. There has been a long-standing controversy as to whether coronal or metric type II bursts originate from CME-driven (piston-driven) shocks and/or from blast-wave shocks (Cliver *et al.*, 1999).

Radio observations of solar type II bursts were first made by ground-based radio spectrographs, operating at metric wavelengths (Wild, 1950). These early observations therefore provided only spectral information on these coronal radio sources. Later, radioheliographs were constructed whose images provided direct information on the spatial locations and heights of the coronal radio sources. Simultaneous imaging by coronagraphs and radioheliographs permitted a comparison of the type II sources with coronal structures seen in white light, albeit in somewhat different spatial regions.

The rest of this section concentrates on recent observations of coronal shocks detected at radio, X-ray, UV and optical wavelengths and their relationships to other solar features. Recent observations of coronal shocks at optical and UV wavelengths have provided unique diagnostics for the dynamics of CMEs and for the physical parameters and processes in coronal shocks.

5.2. Shocks in the Corona: Metric Type II Bursts and Coronal Waves

An example of a metric type II radio burst is illustrated in Figure 7. This figure shows a dynamic spectrum, which is a plot of the radio intensity as a function of frequency and time. The metric type II burst appears as relatively narrow banded spectral features that drift slowly to lower frequencies with time. The spectral characteristics of metric type II bursts can often be very complex (see Nelson and Melrose, 1985

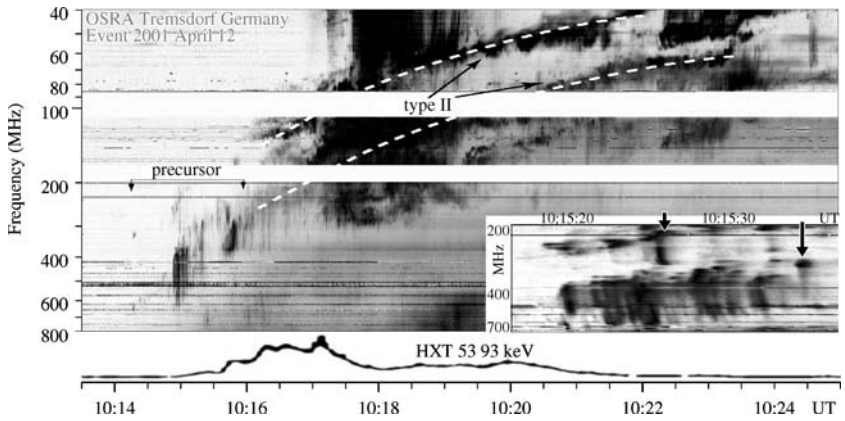

Figure 7. Dynamic radio spectrum and hard X–ray emission (53–93 keV) of the event on 12 April 2001. The event starts with a harmonic type II precursor, followed by a type II burst with multi-lane structure. The "backbone" of the fundamental and harmonic type II emissions is indicated by the white dashed curves. The precursor is cotemporal with the hard X–ray emission (lower panel) and consists mainly of sequences of fast reverse slope (RS) drift bursts, details of which are evident on the expanded time scale spectrum shown in the insert on the right (two of the RS bursts are indicated by the arrows) (adapted from Klassen *et al.*, 2003).

and Mann, 1995 for reviews). In addition to a common fundamental-harmonic band structure, the metric type II bursts also typically exhibit band splittings, multiple lanes and sometimes a so-called herringbone structure.This structure appears as a series of rapidly drifting, short-duration bursts that can drift to higher or lower frequencies. The frequency drift corresponds to the "backbone" of the herringbone structure. While such type II spectral features provide evidence of a coronal shock wave, they do not directly yield unambiguous information on the nature and origin of the shock.

In 1960, solar Hα observations revealed the existence of flare-associated waves, known as Moreton waves, that appeared as arc-shaped fronts propagating away from the flare site at speeds of the order of 1000 km s^{-1} (Moreton, 1960). The origin of these waves was attributed to a shock propagating through the corona, while sweeping over the chromosphere (Uchida, 1960). Noting that type II radio bursts were closely associated in time with Moreton waves, Uchida (1974) unified the interpretation of type II bursts and Moreton waves by demonstrating that both could be simultaneously produced by a propagating "weak" fast-mode shock. The observed slow frequency drift of the type II emission was interpreted as radiation generated by the plasma emission mechanism as the shock propagated through the decreasing coronal density. In Figure 7, the two drifting bands (outlined by the white dashed curves), with a frequency ratio close to 2, correspond to type II radiation generated in the corona at the fundamental and harmonic of the plasma frequency.

It was originally believed that the MHD shock that generated these metric type II bursts were blast-wave shocks produced by an associated solar flare. When CMEs were first discovered (Tousey, 1973), it was then suggested that these metric type II bursts might in fact be generated by the piston-driven shocks associated with CMEs (Gosling *et al.*, 1976). To compare the location or height of the radio source with the white-light CME, it was necessary to use a coronal density model (e.g. Saito *et al.*, 1970) to convert an observed radio frequency to its corresponding coronal height. It was also necessary to extrapolate the observations from the spatial region of the metric type II burst (in the low corona) to the spatial region of the coronagraph observations (in the high corona). To match the coronal shock dynamics implied by the frequency drift rate of the type II radio emissions to the CME dynamics derived from the coronagraph observations, it was found necessary to conclude that the metric type II bursts were generated in enhanced density regions in the corona (Robinson and Stewart, 1985). One possible way out of this dilemma was to assume that metric type II bursts were produced by distinct coronal blast-wave shocks that were not directly related to the CME and its associated shock (Wagner and MacQueen, 1983). However, Steinolfson (1985) suggested an alternative explanation, namely that the type II radio sources were generated along the flanks of the CME-driven shock. (For a possible direct optical detection of a shock along the flank of a CME, see Vourlidas *et al.* (2003) and Section 5.5).

Spectral analyses depend critically on the density model. With the development of radioheliographs, radio images were obtained which could be directly

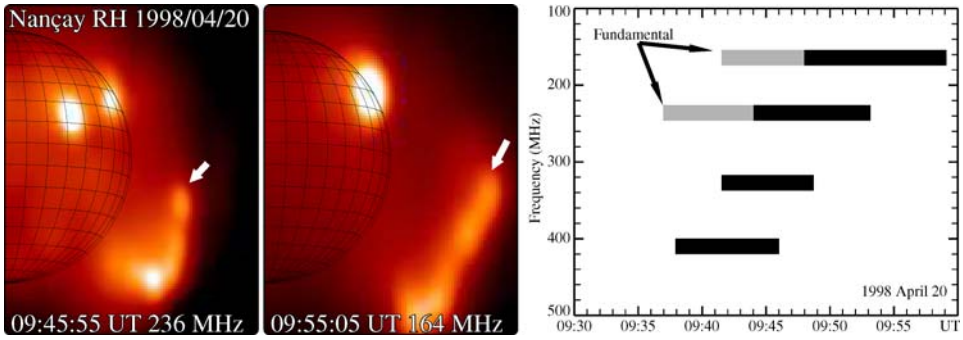

Figure 8. April 20, 1998 event. (a) NRH images showing the outward progression of a weak type II-like radio source (indicated by the arrows) in the southwest quadrant at two different frequencies. (The source in the northwest quadrant is a stationary noise storm). (b) A radio spectrum constructed from consecutive images of the type II-like radio sources (adapted from Maia *et al.*, 2000).

compared to the white-light images for the limb events and no assumption about a coronal density model was necessary. In general, comparisons between radio and coronagraph image data from the Solar Maximum Mission (SMM) and more recently from SOHO/LASCO have indicated that the type II burst sources were often located well below the CME leading edge (Gergely *et al.*, 1983; Pick, 1999), who listed most of the relevant analysis performed with Clark-lake, Culgoora and Nançay radioheliographs.

However, Maia *et al.* (2000) observed a few events in the Nançay Radioheliograph (NRH) images where type II-like signatures exhibited the properties expected for a CME-driven shock. They found sources that move radially outward and closely match both the position and velocity of the CME leading edge. One of the best cases is shown in Figure 8. The CME on 1998 April 20 was fast ($>$1400 km s^{-1}), and as such one would expect a shock associated with this event to develop in the corona at relatively low altitudes. Figure 8 (left) shows images of an extended radio feature at two NRH frequencies at about the time that the CME, observed later by LASCO, was propagating through this region of the corona. Its leading edge, measured at 10:07 UT and extrapolated to the time of the NRH image at 164 MHz, coincided with the location of the radio feature. Observed at four NRH frequencies, the extended radio sources moved radially outwards with an initial projected velocity of about 1000 km s^{-1}. A spectrum constructed from the observations at these frequencies is shown in Figure 8 (right). The regions shown in gray at 164 and 236 MHz correspond to weaker emissions. A large increase in intensity was later observed, at about the time where the black regions in the figure first appear. This spectrum of the outward moving radio feature is clearly type II-like, with evidence for radio emissions at both the fundamental and harmonic (compare with Figure 7).

Multi-wavelength coronal studies, based on imaging observations in EUV, X-ray, Hα and radio, have significantly improved our understanding of the origin and

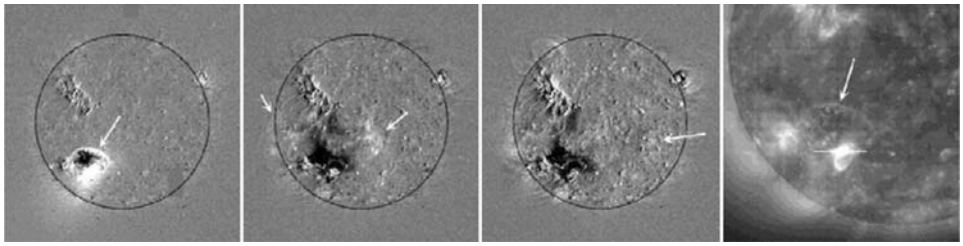

Figure 9. Example of an EIT wave from September 24 1997. The first three panels show successive images at 02:49, 03:03 and 03:23 UT with a pre-event image digitally differenced from them. Arrows indicate the EIT- wave front(s). The last panel shows a subfield of the first panel (undifferenced), showing an example of a sharp brightening (from Biesecker *et al.*, 2002).

nature of the shocks producing type II radio emissions. There is mounting evidence to suggest that many, if not most, metric type II bursts are produced by coronal shocks that are probably not the pure blast waves originally envisioned by Uchida (1974).

An important factor in this new understanding was the discovery of the large-scale coronal EUV (EIT) and SXT waves by the SOHO/EIT and Yohkoh/SXT telescopes, respectively. The EIT waves (Thompson *et al.*, 1998) typically appear as diffuse brightenings propagating away from the site of active regions; their speeds, which are difficult to accurately determine due to the poor temporal cadence of the observations, appear to be a few hundreds of km s^{-1}. An example of an EIT wave is shown in Figure 9. The exact nature of these waves is not yet fully understood. EIT waves have a strong association with CMEs (Biesecker *et al.*, 2002) and often with EUV dimmings, which are usually restricted to the region traced by the transit of Moreton waves. Biesecker *et al.* (2002) established that EIT waves are not generally well correlated with type II bursts, except a small subclass ($\sim$7%) that have sharp bright fronts. They proposed that these sharp wave fronts may be the coronal counterpart of Moreton waves.

This suggestion was confirmed for a few events for which EIT and Moreton waves and type II-like bursts appeared in close spatial and temporal coincidence (Pohjolainen *et al.*, 2001). Moreover, this and subsequent studies established that, for this class of flare/CME events, the observed latitudinal expansion of the CME was directly related to the propagation of the Moreton wave. This suggests that the coronal shock triggers destabilization and magnetic interaction of coronal structures as it propagates through the corona. Examining this correlation more carefully, Warmuth *et al.* (2004) found that all EIT waves with sharp wave fronts decelerated with the rate of deceleration decreasing with increasing time and distance. They pointed out that the characteristics of these coronal waves, their rapid deceleration, the broadening of the intensity profile and the decrease of amplitude with increasing distance and time, are characteristics of blast waves, rather than piston driven shocks. Additional evidence was provided by Khan and Aurass (2002), Narukage

et al. (2002) and Hudson *et al.* (2003) who showed that the coronal waves detected by the Yohkoh/SXT telescope also have the expected relationship to Moreton waves and type II bursts. These analyses of the wave propagation, especially of directional changes, led them to conclude that the disturbances were blast waves related to a flare and they argued that the type II burst was generated by the same blast wave.

However, not all observations of type II emission are consistent with pure blast waves. Klein *et al.* (1999) observed a type II source to appear above an expanding soft X-ray loop in SXT images, while a neighbouring loop did not change. This difference between the loops suggested that the proximity of the type II source and the expanding loop was not coincidental, but that the expanding loop outlined a peculiar magnetic structure which was the driver of the type II emitting shock wave. A second argument against a pure blast wave picture is the statistical result by Pearson *et al.* (1989) who found no significant indication that the type II producing flares were particularly impulsive. These findings suggest that type II shocks are initially not pure blast waves, although they may become blast waves during the course of the event. The frequent observation of type II radio precursors also suggests that the type II shocks are initially piston driven (Klassen *et al.*, 1999, 2003). Indeed, such precursor spectral signatures (illustrated in Figure 7) occur during the impulsive flare phase and consist of sequences of fast-drift bursts or pulsations whose overall frequency envelope drifts at a normalized drift rate. This rate is similar to that of the subsequent metric type II burst, and it typically displays a similar harmonic structure. The fast-drift bursts that constitute the precursor trace the propagating disturbance before it excites type II emissions. This implies the existence of electron beams that propagate towards the expanding loops and the hard X–ray (HXR) sources. Klassen *et al.* (2003) found that the precursor of the event shown in Figure 7 was associated with an expanding loop system, with speeds of expansion that varied from 200 to 700 km s^{-1}. They suggested that the type II precursor is a signature of a moving reconnection process that occurred above the expanding soft X–ray loops, which drive the precursor and generate the subsequent type II burst.

5.3. The Link between the Corona and the Interplanetary Medium: Decametric-Hectometric Type II Bursts

The above discussions demonstrate the difficulty of determining conclusively whether a given coronal shock, detected solely by its ground-based radio signatures, is a piston-type shock being driven by the CME (or an associated small-scale disturbance) or is instead an undriven blast-wave shock associated with a flare. Another approach that may help to resolve the blast wave versus CME-driven shock controversy is to establish the relationship of the coronal type II bursts to their low-frequency counterparts that are observed by radio receivers on interplanetary

spacecraft (see Forsyth *et al.* 2006, this volume). It is well established that these counterparts are directly driven by CMEs (Cane *et al.*, 1987).

An important observational advance was provided by the radio receivers of the WAVES experiment on the Wind spacecraft, which for the first time observed solar radio emissions at high-frequency and high-time resolution in the decametric-to-hectometric (D-H) wavelength band from 1 to 14 MHz. Leaving only a relatively small frequency gap between the spaceborne and ground-based radio observations, the Wind/WAVES observations offer a unique opportunity to establish the possible causal relationship between the coronal (metric) type II bursts and the interplanetary (kilometric) type II emissions. However, since imaging at these low frequencies is not possible, only spectral comparisons can, at present, be made.

When Wind was launched in 1994, during solar minimum, no solar type II radio emissions were observed in the D-H band, although during that time many metric type II bursts were observed by ground-based observatories. This led Gopalswamy *et al.* (1998) to conclude that the metric type II bursts were produced exclusively by blast-wave shocks, associated with flares, that did not propagate into the high corona and interplanetary medium. However, by 1997, as the maximum of solar cycle 23 approached, distinct slow frequency-drifting type II emissions began to appear in the D-H wavelength range and they became more abundant as solar maximum was reached (Kaiser *et al.*, 1998; Gopalswamy *et al.*, 2000). The spectral characteristics of these D-H type II bursts were quite diverse and were usually observed in association with major flares associated with fast CMEs.

It was found that these D-H type II bursts often naturally extended to the low-frequency kilometric type II emissions, known to be generated by CMEs (Reiner and Kaiser, 1999b; Reiner *et al.*, 2000a, 2003). However, it was more difficult to establish unequivocally their causal relationship to the metric type II bursts, partly because of the frequency gap (14–20 MHz) to the ground-based observations (Reiner *et al.*, 2000a; Gopalswamy *et al.*, 2000; Reiner *et al.*, 2003). The best way to establish this causal relationship is to require that the dynamics implied by the observed frequency drift rates of the metric and decametric type II bursts should agree, i.e., a metric type II burst is related to a decametric type II burst if and only if both the frequency drift rate *and* the projected origin time in these two frequency regimes correspond. Since the frequency drift rate of the type II burst depends on the frequency, this of necessity can only be done within the context of a coronal density model. However, if it is found that their frequency drift rates are a continuation of each other over a significant time period and frequency range, then one can be reasonably confident that the metric and decametric type II emissions were produced by the same coronal shock.

An example is illustrated in Figure 10. The D-H type II emissions and a metric type II burst, which were observed over a particularly wide frequency range, are shown in the (space-based) WAVES and (ground-based) Culgoora dynamic spectra, respectively. Also shown in Figure 10 are the height-time measurements for the

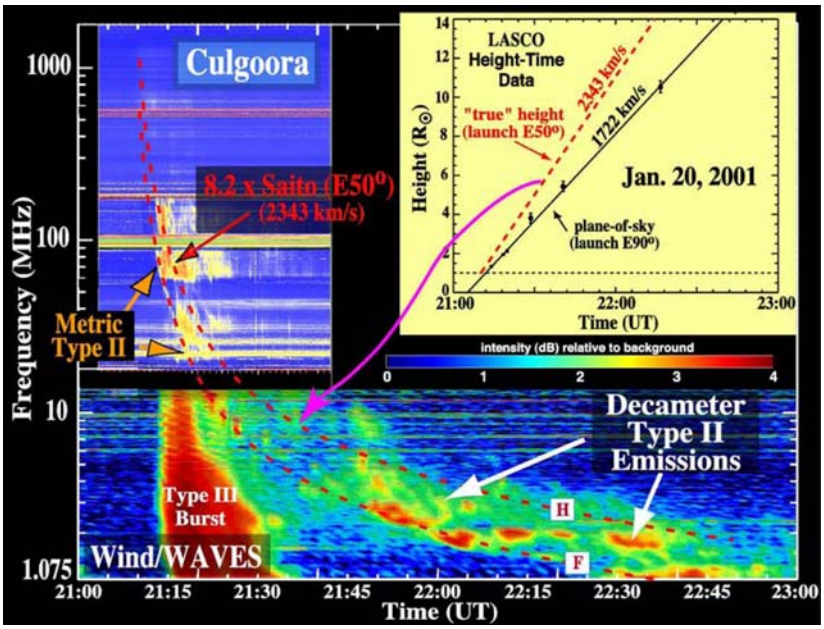

Figure 10. Dynamic spectra showing the decametric and metric frequency-drifting type II radio emissions associated with the 20 January 2001 CME event. The measured CME height-time data were used to obtain a frequency-time track, which was then simultaneously fit to the frequency drift of the metric and decametric type II radio emissions. It was found that to get a good fit it was necessary to assume a CME launch angle of E50° with an enhanced Saito coronal density model, suggesting that the radio emissions originated in high density streamers (adapted from Reiner *et al.*, 2003a).

corresponding LASCO CME. By requiring consistency between the frequency drift rate of the type II radio emissions and the height-time data from the CME, Reiner *et al.* (2003) were able to fix the scale of the coronal density model (Saito *et al.*, 1970) and to establish, within the context of this model, that the frequency drift of the D-H emissions was a continuation of the frequency drift of the metric type II emissions, as indicated by the red dashed curves in Figure 10. Thus, at least for this event, the metric and D-H type II emissions were both generated by the same CME-driven shock, which must have formed very low in the corona, in agreement with the results of Maia *et al.* (2000). Dulk *et al.* (1999) using a similar approach reached similar conclusions. By contrast, there are other cases where, using the same technique, it was found that the metric and D-H type II emissions were not dynamically related (Reiner *et al.*, 2000a).

5.4. Coronal Shock Interactions

Shocks in the corona can also interact with coronal structures. The propagating CME-driven shocks are often observed to deflect coronal streamers and to interact

with coronal material from a preceeding CME (see Schwenn *et al.* 2006, this volume). These shock interactions can also have radio consequences (Gopalswamy *et al.*, 2001).

Mancuso and Abbo (2004) presented a rare observation of a type II burst associated with an X20 flare on April 2, 2001 accompanied by a very fast (>2000 km s^{-1}) CME. The type II emission appeared at frequencies near 100 MHz and subsequently drifted toward both higher and lower frequencies. Mancuso and Abbo (2004) modeled this event as the result of the CME shock impact on a streamer at some distance above the solar surface, and, as the CME *encountered* the streamer, shocks moved both up and down along the streamer axis. The SOHO/LASCO and SOHO/UVCS observations supports this model. This observation demonstrated that type II emission does not necessarily occur at the outermost part of a CME, but can arise from the CME flanks if conditions are right. Emission from a streamer suggests that high density or perhaps relatively high plasma β may be important in determining which parts of the shock produce radio emission. The analysis of Reiner *et al.* (2003) also suggest that the type II emissions may be generated in portions of the shock that pass through the coronal streamers.

5.5. Optical Observations

Direct optical observations of shocks associated with CMEs are very difficult and at best can only be achieved in rare situations, but they can be made at heliocentric distances of a few solar radii where shocks are expected to form. A major difficulty is discriminating between plasma compressed by a shock and plasma compressed by an expanding magnetic structure.

The best direct white-light observation of a CME/shock is that of Vourlidas *et al.* (2003) (for details see Schwenn *et al.* 2006, this volume). A 800–1000 km s^{-1} jet-like CME (about 20° opening angle) on 1999 April 2 showed an extremely sharp edge, as expected for a shock, and its shape was that expected for a bow shock driven by a jet. While there was no reported type II radio emission to confirm the shock interpretation, this CME produced a clear deflection of a streamer when the "shock" reached it and Vourlidas *et al.* (2003) provided a simulation to support their interpretation of the sharp white-light feature as a fast-mode MHD shock.

5.6. Ultraviolet Observations

There have also been about 10 detections of CME-driven shocks in the ultraviolet with SOHO/UVCS (Ciaravella *et al.*, 2006). Raymond *et al.* (2000) observed an event on 1998 June 11. Its speed was 1200 km s^{-1} based on LASCO images and the timing of the event seen at $1.75 R_{\odot}$ by UVCS. Furthermore, a type II burst was observed at Nançay during the time that the event was seen by UVCS, and the density obtained from the type II frequency agreed with the pre-CME density obtained from

the ratio of O VI emission lines. Both the type II frequency width and the observed brightening in O VI and Si XII lines indicated a modest compression. The O VI line profile obtained by UVCS implied an oxygen kinetic temperature much higher than the proton temperature, as has been observed in heliospheric shocks (Berdichevsky *et al.*, 1997) and supernova remnant shocks (Raymond *et al.*, 1995; Laming *et al.*, 1996). Raymond *et al.* (2000) noted that Wind/WAVES observed type II emission simultaneous with that observed at Nançay, but 6 times lower in frequency, implying a density nearly 40 times smaller. The UVCS density, and therefore the Nançay type II emission, pertain to the streamer that lay directly above the CME site. The Wind/WAVES emission probably originated in the lower density region between the streamers to the southeast of the CME axis. Another possible interpretation is that Wind/WAVES emissions corresponded to a shock that originated earlier. It is also interesting that the shock speed estimated from the Nançay frequency drift rate and models of the average coronal density was only about half the speed obtained from LASCO, even though the density agreed with that obtained by UVCS. This was attributed to the difference between the actual streamer density distribution and the average coronal models, but perhaps non-radial motion of the section of the shock that produced type II emission also affected the velocity estimate. However, the type II drift rate in this complex event is uncertain.

Mancuso *et al.* (2002) observed another SOHO/UVCS event on 2000 March 3 that produced type II emission observed at Hiraiso, Culgoora and Bruny Island simultaneous with the appearance of the shock in the UVCS spectrograph slit at $1.5R_{\odot}$. The UVCS data is shown in Figure 11. The densities inferred from the type II frequency and UVCS line ratios obtained in an earlier synoptic scan were in

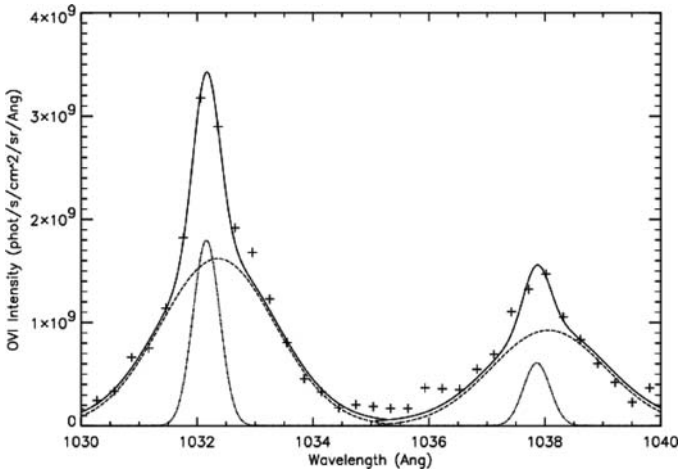

Figure 11. O VI 1032, 1037 Å doublet detected on March 3, 2000 during the passage of the shock front. The $1/e$ width of the shocked material indicates a speed of 400 km/s as compared with 70 km/s of the unshocked pre-CME corona (adapted from Mancuso *et al.*, 2002).

agreement at 1.2 to 1.5 $\times$ 10^7 cm^{-3}. The shock speed obtained from the frequency drift and the pre-CME density structure obtained from UVCS was 1100 $km\,s^{-1}$, in reasonable agreement with the 920 $km\,s^{-1}$ speed observed by LASCO in the plane of the sky. The Bruny Island radio data suggests that the type II drift rate has been overestimated by as much as 25% in this complex event, which would still be in reasonable agreement with the LASCO speed. As for the 1998 June 11 event, the compression was a modest factor of 1.8 as estimated from type II frequency splitting and UVCS observed strong broadening of the O VI emission lines. The O VI line widths agreed well with the expected velocity width for the observed shock speed and compression ratio in the model of Lee and Wu (2000). While the radio and UV observations are remarkably consistent, the lack of an interplanetary shock signature from Wind/WAVES leaves open the possibility of a blast wave origin for the type II emission.

An important application of UV data to the study of shocks is the derivation of pre-CME density structures for use in shock speed estimates. They can also be used to derive magnetic field limits from the requirement that for a piston-type shock to appear the CME speed must exceed the fast mode speed. This yielded lower limits to the plasma β at 1.9 $R_\odot$ of 0.01 to 0.47 for 37 radio bursts observed in 1999. Similarly, during the 2002 April 21 X1.5 class event, the lack of type II emission until after the CME passed the UVCS slit at 1.63$R_\odot$ gave a lower limit to the magnetic field at this height of 1 G (Raymond *et al.*, 2003).

6. Radio Diagnostics of Coronal Electron Acceleration and In-Situ Electrons

M. REINER, D. MAIA, H. CANE, L. K. KLEIN

6.1. INTRODUCTION

Solar radio emissions are diagnostics of the acceleration of coronal electrons from suprathermal to relativistic energies. These remote electromagnetic signatures of coronal electrons, observed at high cadence in dynamic spectra and in images, provide information on the precise timing of solar acceleration processes. They also provide information on the locations and physical characteristics of the electron acceleration sites and their relationships to coronal structures. The number and diversity of these radio sources, extending from millimeter to decameter wavelengths, suggest a wide variety of coronal acceleration processes related to solar energetic events observed in white-light, EUV, and X-rays. Some of these accelerated electrons are trapped in closed coronal magnetic structures, while others freely escape along open magnetic field structures into interplanetary space, where they can be observed in situ. These remote radio observations can facilitate tracing the in-situ signatures of solar energetic particles back to their solar origin.

Recent multiwavelength observations indicate that, for a given solar event, different populations of energetic protons and electrons may be accelerated by different physical mechanisms at different times and from different coronal sites. Until recently, the prevalent view was that large SEP events, observed in interplanetary space, were the exclusive result of particle acceleration at the bow shock of CMEs. However, from the association of both CMEs and radio emissions observed at low coronal altitudes with the complex radio emissions observed in the 1–14 MHz range, there is now ample evidence to suggest that coronal processes can also contribute to the SEP production (see also Klecker *et al.*, 2006, this volume). We focus here mainly on the solar origin of near-relativistic impulsive electron events. For these events, the release time at the sun can be accurately determined and directly compared to the various radio signatures. The inferred solar injection times of these near-relativistic in-situ electrons are often found to be significantly delayed with respect to the radio signatures generated by the low-energy electrons in the corona.

6.2. Diverse Radio Diagnostics of Electron Acceleration in the Corona

We discuss here those radio signatures that are necessary for understanding the causal link between energetic electrons in the corona, detected by their remotely observed radio signatures, and those detected in situ in the interplanetary medium.

6.2.1. *Persistent Sources of Suprathermal Electrons*

Interplanetary type III radio storms detected at kilometric wavelengths are closely related with noise storms at metric wavelengths, which are a common form of activity observed in the absence of flares (Bougeret *et al.*, 1984; Kayser *et al.*, 1987). These storm emissions are related to the dynamical evolution of the coronal magnetic field (Bentley *et al.*, 2000), and at onset, are located in regions of coronal restructuring observed in white light (Kerdraon *et al.*, 1983) or in soft X-rays (e.g. (Lantos *et al.*, 1981). Type III storms can persist for days and likely contribute to the population of electrons extending to 2 keV in the interplanetary medium.

6.2.2. *Radio Emission from Electron Beams*

Solar type III radio bursts are observed over a very wide range of frequencies ($\geq$1 GHz – 10 kHz) and are emitted by $\leq$20 keV electrons accelerated at the sun, at various altitudes (sometimes as high as $1 R_{\odot}$). These electron beams have access to open field lines that allow them to escape into interplanetary space, where they can be detected in situ as impulsive electron events (Lin, 1998). Metric type III bursts generally consist of groups of individual bursts (typically tens of bursts over a period of one or more minutes) that overlap and merge at decreasing frequencies so that by $\sim$1 MHz they generally appear as a single burst with a typical duration

of ∼5 minutes. Metric type III bursts are generally not well correlated with hard X-ray (HXR) emissions (Kane, 1981), although when both emissions are associated, the temporal correlation is excellent, indicating a common source of electron acceleration (Raoult *et al.*, 1985).

6.2.3. *Type IV Bursts*

Type IV bursts generally consist of a broadband continuum that can extend from several GHz to ∼10 MHz, and are most often associated with large flare/CME events (see Schwenn *et al.* 2006, this volume). Type IV continua are often associated with gradual HXR bursts, and are generally followed by a post-gradual emissions (stationary type IV bursts) that may last for tens of minutes to hours after the end of the HXR and microwave emissions. Such long lasting radio emission is a signature of the acceleration of suprathermal electrons in the middle corona, continuing for hours after the flare (Trottet, 1986). Moving type IV sources are due to suprathermal to MeV electrons injected into expanding magnetic arches, behind the CME leading edges. Some other narrower type IV moving sources are often associated with eruptive prominences.

6.3. Complex Type III-Like Bursts at D-H Wavelengths

While many type III radio bursts have simple, well-defined intensity-time profiles at hectometric wavelengths, a significant number of type III events are very intense, complex and of long-duration at decametric-to-kilometric wavelengths. First identified and studied in the 1980's, it was noted that they had a good temporal correspondence with the metric type II bursts, leading (Cane *et al.*, 1981) to suggest that the electrons that produced these complex type III bursts were accelerated by coronal shocks (and they were therefore called shock associated (SA) events). On the other hand, some authors noted that the durations of the complex type III bursts were similar to those of associated continuum radio and HXR emissions, and argued in favor of a low corona electron acceleration process (Kundu and Stone, 1984; Klein and Trottet, 1994). Nevertheless, it was commonly accepted, from supporting statistical studies (Kahler *et al.*, 1989), that the complex type III events were generated by electrons accelerated at coronal shocks.

Cane *et al.* (2002) noted that some complex type III events had clear metric type III emissions at frequencies higher than those of the corresponding type II burst and Reiner *et al.* (2000b) demonstrated that for some complex type III-like events there was a good temporal correspondance between the duration and intensity variations of the time profiles of the hectometric and decimeter/microwave emissions at 1–3 GHz, as illustrated in Figure 12. This correspondence suggests that both emissions were generated by different electron populations accelerated in the lower corona over extended time periods. Reiner and Kaiser (1999a) reported that the radiation characteristics of the complex type III-like emissions observed at high time and frequency resolution in the D-H range (1–14 MHz) (see Figure 12) were quite

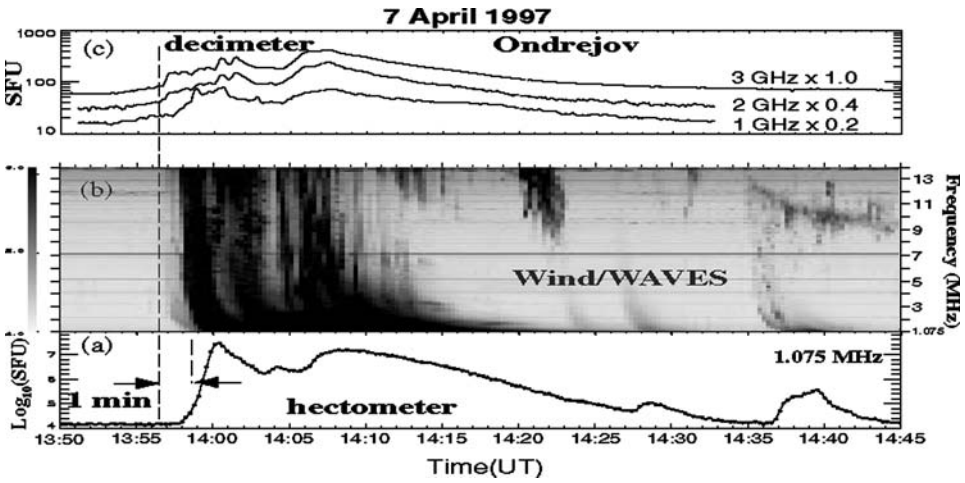

Figure 12. Comparison of the complex type III burst observed on 1997 April 7 by Wind/WAVES in the frequency range from 1 to 14 MHz, with the radio emissions observed by the Ondřejov observatory from 1 to 3 GHz. Note the similarity in the shape and duration of the intensity-time profiles in these widely separated frequency regimes (adapted from Reiner *et al.*, 2000b).

unusual and suggested that some of these complex radiation characteristics might be related to the electron beams propagating through the highly disturbed corona behind the associated CME. Reiner *et al.* (2001) observed that these complex type III-like emissions were usually associated with major flare/CME events, while (Cane *et al.*, 2002) showed that >20 MeV SEP events were associated with a class of long-duration type III bursts (called type III-*l*), which include the complex type III-like bursts discussed here. Nevertheless, although many of these intense complex type III bursts are most likely generated from electrons accelerated low in the corona, there may still be some that result from electrons accelerated by coronal shocks (e.g. Bougeret *et al.* 1998).

6.4. Coronal Radio Diagnostics of "Delayed" In-Situ Electrons

A different approach to inferring the origin of solar electrons is based on the analysis of in-situ electrons observed by spacecraft. Systematic studies on the relative timing of coronal electron release and of associated phenomena (Krucker *et al.*, 1999; Haggerty and Roelof, 2002) found that the inferred solar release times of electrons could be significantly delayed relative to the onset of the type III burst that result from the escape of suprathermal electrons into interplanetary space. Such delays, ranging from 0 to more than 40 minutes, are quite inconsistent with the expectation that the electron beams detected in situ should be the generators of the type III radiation (Lin *et al.*, 1973).

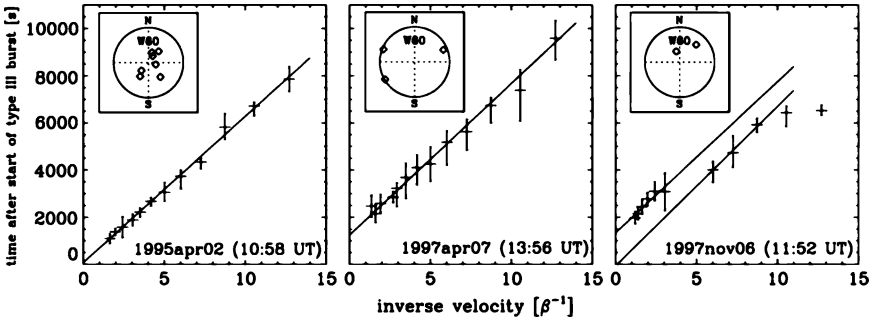

Figure 13. Illustrative examples of the three different classes of in-situ impulsive electron events that have very different velocity dispersion characteristics. In all cases, the light propagation time of 8.3 minutes was added to permit direct comparison of the injection times with the times of the observed remote radio emission at 1 AU (adapted from Krucker *et al.*, 1999).

The Krucker *et al.* (1999) study, which analyzed suprathermal to near-relativistic impulsive electrons, found that impulsive electron events could be classified into three categories depending on the characteristics of the observed velocity dispersion in the beam made evident on $1/\beta$ plots such as illustrated in Figure 13. First, the onsets at all energies lie on the same straight line with an inferred release time that coincides with the onset of the type III radio emissions. Second, the onsets at different energies all lie along the same straight line but the inferred injection time is significantly delayed relative to the onset time of the type III radiation. Third, the low-energy electron velocity dispersion extrapolates to a time that coincides with the onset time of the type III radio emissions, while the velocity dispersion of the high-energy (near-relativistic) electrons extrapolates to a solar injection time delayed by up to 40 minutes from the type III emissions. Explanations advanced for this phenomenon can be divided into two major categories: (1) the "delays" reflect distinct coronal acceleration processes (multiple populations), (2) the "delays" result from propagation effects in the interplanetary medium (single population).

6.4.1. *Multiple Populations*

Krucker *et al.* (1999) found good agreement between the nominal Parker spiral length, based on the measured solar wind speed, and the path length deduced from the measured velocity dispersion in the electron onset times at different energies (the so called $1/\beta$ method – see Figure 13). This led them to conclude that the delays observed in the times of the first-arriving electrons were not due to propagation effects but rather reflected differences in the timing of the electron acceleration at the Sun. They thus proposed that the delayed in-situ electrons corresponded to a population of electrons that were released at the Sun (without producing a type III burst) later than the suprathermal electrons (which were not detected in situ) that generated the type III radiation. Based on the correlation they found with the occur-

rence of EIT waves (see Schwenn *et al.* 2006, this volume), Krucker *et al.* (1999) suggested that EIT waves were somehow at the origin of the phenomenon. Klassen *et al.* (2002), on the other hand, found a temporal association of the near-relativistic electron events with coronal shocks (type II bursts) that had associated CMEs.

Simnett *et al.* (2002) also favored a multiple population scenario but regarded any low-corona association as a secondary effect. Based on trends observed between the CME speeds and the corresponding electron fluxes, spectral hardness and delays, they suggested that most of the near-relativistic electrons were accelerated by the CME-driven shock (possibly from a seed population) and were released at a distance from 2 to $3R_{\odot}$.

From in-situ observations near 1 AU, it is known that shocks can accelerate electrons to keV energies and possibly tens of keV, but there is no information on the efficiency of shock acceleration closer to the Sun. Furthermore, arguments on efficiency of electron acceleration to near-relativistic energies by coronal shocks are not conclusive: Mann and Luehr (1994) claim that it should be possible under special conditions, while (Klein *et al.*, 2003b) argued that estimates on the numbers and energy content of type II shock-accelerated electrons between a few keV and several tens of keV remain inconclusive in terms of proving or disproving electron acceleration to high-energies by coronal shocks.

The complexity of coronal processes may also play an important role in the "delays". Detailed studies for all of the Haggerty and Roelof (2002) events for which there were imaging observations from the Nançay Radioheliograph (NRH) were conducted by Pick *et al.* (2003) and Maia and Pick (2004). They identified two classes of electron events: radio-simple (events associated only with type III bursts) and radio-complex (events associated with broadband continua and/or coronal type II bursts). The radio-simple events were either not associated with CMEs or associated with slow CMEs, while the radio-complex events were associated with fast CMEs (velocity in general exceeding 800 $\mathrm{km\,s^{-1}}$). The inferred release times for the in-situ impulsive events associated with radio-simple emissions fell within the time of the metric type III group. An example of a radio complex event, with complex type III emission at decametric frequencies and multiple moving sources at metric frequencies is shown in Figure 14. For the radio-complex events, the inferred release times for the near-relativistic electrons did not generally occur within the type III burst group, but, more significantly, were always close to the start or times of abrupt modifications during the development of the radio event, providing evidence for new sources of coronal acceleration at heights below $1R_{\odot}$. The simplest interpretation of these analyses is that the delayed acceleration of the near-relativistic electrons results from coronal restructuring at variable heights behind the leading-edge of the CME. For some events a new site of electron acceleration may have been triggered by a shock, consistent with the association with EIT waves found by Krucker *et al.* (1999). Similar conclusions were independently reached from preliminary results using NRH and Wind/3DP observations (Klein *et al.*, 2003a).

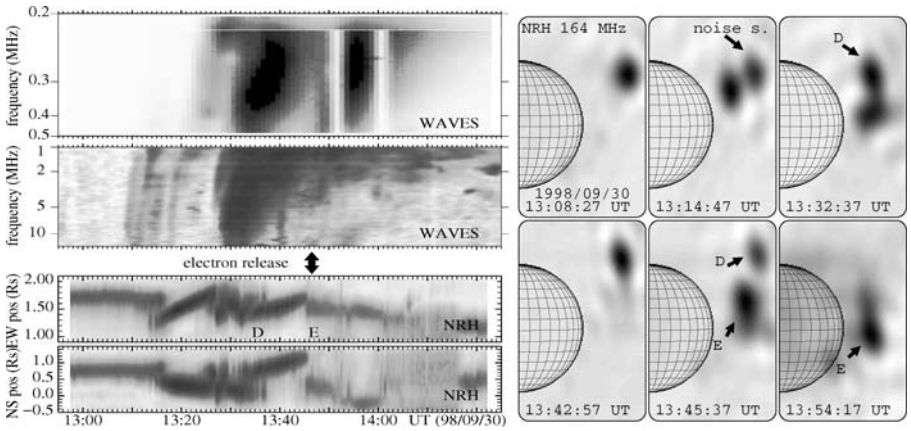

Figure 14. 1998 September 30. (left) Comparison of the emission observed by the NRH (bottom) and WAVES (top). The vertical white bands seen in in WAVES spectrum are due to the saturation. The one-dimensional plot shows a series of radio sources. D marks a moving continuum, followed by a stationary labeled E. The arrow indicates the inferred release time at the sun for the electrons with energies above 100 keV. Note that this time coincides with the sudden disappearance of D, the onset of E, and with the low frequency type III burst detected by WAVES. (right) Panel of images showing the positions of the sources seen by the NRH (adapted from Maia and Pick, 2004).

6.4.2. *Single Population*

Cane (2003) made a careful analysis of the interplanetary type III bursts, associated with the Haggerty and Roelof (2002) electron events, whose spectral shape, near the local plasma frequency at the spacecraft, is indicative that they are emitted close to the spacecraft. Cane (2003) found that the "radio drift times" (the time interval from the onset of the type III to the time when the emission extrapolates to the plasma line) appear to correlate with the electron "delays" and that the electron delays tend to be longer for higher local plasma density. The author argues that the simplest explanation for these correlations is that the energetic in-situ electrons, and the ones at the origin of the type III burst, are of the same population, and that the observed delays arise from underestimating the particle propagation times. These analyses disagree with the $1/\beta$ analyses which assume a scatter-free propagation path in the solar wind. Reconciliation of the disagreement between the two techniques is a topic for future investigation.

7. Summary

T. FORBES, G. MANN, M. PICK

Since CMEs originate in the low solar corona, understanding the physical processes that generate them is strongly dependent on coordinated multi-wavelength

observations. Observations in white light, radio, optical lines, UV, and X-rays have already established that most, but not all, CMEs are accelerated within a solar radius of the surface of the Sun. It has also been shown that CMEs are typically associated with the formation of X-ray loops and chromospheric ribbons, which may, or may not, be bright enough to constitute a classical flare. However, many questions concerning the origin of CMEs remain to be answered. For example, the processes that build-up stresses in the coronal magnetic field, as well as the processes that lead to the destabilization of this field have not yet been determined.

The multi wavelength observations of the last decade have confirmed that reconnection plays a key role in the relaxation of the magnetic field disrupted by a CME. During a CME, magnetic field lines mapping from the ejected plasma to the photosphere are stretched outward to form a current sheet in which field lines reconnect to form closed, magnetic loops. During the reconnection process, power extracted from the magnetic field drives flows and heats the plasma. Much of the released energy is channeled down to the solar surface and leads to the heating and evaporation of the chromospheric plasma. Although the occurrence of reconnection in the aftermath of CMEs has now been firmly established, whether reconnection also plays a significant role before, or during, the onset of a CME remains unknown. Observations of small to moderately sized flares suggest that reconnection can trigger the eruption of fast CMEs. Much of current research is focused on looking for reconnection signatures just before onset. We anticipate that as more information is gathered about the flows and heating produced by reconnection in the corona, we will eventually learn how rapid reconnection occurs and what the dominant physical processes are.

Opening of transequatorial loops typically occurs during the development of large-scale CMEs. The opening of the loops leaves a region dimmed in EUV and multiple loop systems are often involved. CMEs reach their full angular extension in the low corona, through successive magnetic field interactions that produce energetic electrons. The associated emitting radio sources spread through the solar disk in a few minutes, much faster than the cadence of the coronagraph instruments. The EUV and Soft X-ray dimmings observed on the disk open the possibility of estimating the mass in these ejecta and of determining the source regions relative to the surface field. The EUV dimmings that are observed result from the removal of the hot coronal material by the CME, so they trace out the footpoints of the magnetic field lines that are opened by the eruption of the field.

What kind of shocks form during a flare or a CME also remains an unanswered question. That shocks do form is without doubt, but how many there are during a given coronal event and whether they are of the blast-wave or driven (i.e. piston-driven) type is still unknown. How these are related to the driven shocks seen in interplanetary space is also not clear. At the moment it appears that type II radio bursts can be generated by different sources. Radio observations suggest that CME-driven shocks can be formed low in the corona. As more data have been obtained the picture seems to have become even more confused in some respects. For example,

the relationship between CME-generated waves seen in UV by EIT to the Moreton waves seen in Hα by ground based observatories is uncertain. A high observing cadence may be necessary to resolve this. The fact that shocks have been rarely detected in white light is not yet fully understood.

It is well known that shock waves are able to accelerate particles to high energies. There are, however, a few doubts that large SEP events observed in the interplanetary medium are the exclusive result of particle acceleration at the bow shocks of CMEs. In this chapter, we restricted our discussion to the current understanding of the origin of energetic electrons. It is well accepted that the appearance of type II radio bursts shows that electrons must be accelerated by coronal shock waves. But, the role that shocks play in the corona in the production of energetic electrons is not clear. This is true for impulsive electron events observed in the interplanetary medium and also for energetic electrons which strike the solar surface. Most of the complex type III events detected at hectometric wavelengths in the high corona, which are also associated with CMEs, appear to be generated from electrons accelerated low in the corona. For these events, as well as for impulsive quasi-relativistic electron events, these electrons might also be generated by the reconnection process in the corona directly, by the reconnection electric field, or indirectly by the turbulence in the reconnection outflows. How these electrons escape into the interplanetary medium is an open question.

During the last decade the availability of high quality data from numerous spacecraft such as Yohkoh, ULYSSES, SOHO, TRACE, Wind, ACE, and RHESSI has deeply changed our picture of the processes occurring on the Sun. Nevertheless, many problems remain unsolved and will require much effort in the future in order to be resolved. This is especially true for CME initiation, the relationship between the primary energy release and shock waves, and the sources of energetic electrons and ions. The launch of Solar-B, STEREO (Solar Terrestrial Relations Observatory), and SDO (Solar Dynamic Observatory) in the near future should lead to a significant advance in resolving these outstanding issues.

Acknowledgements

We wish to thank Prof. Frank McDonald for useful comments. T.G. Forbes' contribution to this work was supported by grants ATM-0327512, ATM-0422764, and ATM-0518218 from the US National Science Foundation; NASA grant NNH05-AA131, and the US Dept. of Defense MURI program on Space Weather.

References

Amari, T., Luciani, J. F., Mikic, Z., and Linker, J.: 1999, *Astrophys. J.* **518**, L57.
Andrews, M.D., and Howard, R. A.: 2001, *Space Sci. Rev.* **95**, 147.

Antonucci, E., Kohl, J. L., Noci, G., Tondello, G., Huber, M. C. E., Gardner, L. D., *et al.*: 1997, *Astrophys. J.* **490**, L183.
Anzer, U., and Pneuman, G. W.: 1982, *Sol. Phys.* **79**, 129.
Asai, A., Yokoyama, T., Shimojo, M., and Shibata, K.: 2004, *ApJ* **605**, L77.
Aschwanden, M. J., Benz, A. O., Dennis, B. R., and Schwartz, R. A.: 1995, *ApJ* **455**, 347.
Bale, S. D., Reiner, M. J., Bougeret, J.-L., Kaiser, M. L., Krucker, S., Larson, D. E., *et al.*: 1999, *Geophys. Res. Lett.* **26**, 1573.
Bentley, R. D., Klein, K.-L., van Driel-Gesztelyi, L., Démoulin, P., Trottet, G., Tassetto, P., *et al.*: 2000, *Sol. Phys.* **193**, 227.
Berdichevsky, D., Geiss, J., Gloeckler, G., and Mall, U.: 1997, *J. Geophys. Res.* **102**, 2623.
Biesecker, D. A., Myers, D. C., Thompson, B. J., Hammer, D. M., and Vourlidas, A.: 2002, *Astrophys. J.* **569**, 1009.
Biskamp, D.: 2000, *Magnetic reconnection in plasmas*, Cambridge, UK: Cambridge University Press.
Bougeret, J.-L., Fainberg, J., and Stone, R. G.: 1984, *A&A* **136**, 255.
Bougeret, J.-L., Zarka, P., Caroubalos, C., Karlický, M., Leblanc, Y., Maroulis, D., *et al.*: 1998, *Geophys. Res. Lett.* **25**, 4103.
Cane, H. V.: 2003, *Astrophys. J.* **598**, 1403.
Cane, H. V., Erickson, W. C., and Prestage, N. P.: 2002, *J. Geophys. Res. (Space Phys.)* 14.
Cane, H. V., and Lario, D.: 2006, *Space Sci. Revs.*, this volume, 10.1007/s11214-006-9011-3.
Cane, H. V., Sheeley, N. R., and Howard, R. A.: 1987, *J. Geophys. Res.* **92**, 9869.
Cane, H. V., Stone, R. G., Fainberg, J., Steinberg, J. L., Hoang, S., and Stewart, R. T.: 1981, *Geophys. Res. Lett.* **8**, 1285.
Chen, J., Howard, R. A., Brueckner, G. E., Santoro, R., Krall, J., Paswaters, S. E., *et al.*: 1997, *Astrophys. J.* **490**, L191.
Chen, J., Santoro, R. A., Krall, J., Howard, R. A., Duffin, R., Moses, J. D., *et al.*: 2000, *Astrophys. J.* **533**, 481.
Ciaravella, A., Raymond, J. C., and Kahler, S. W.: 2006, *Astrophys. J.* submitted.
Ciaravella, A., Raymond, J. C., Li, J., Reiser, P., Gardner, L. D., Ko, Y.-K., *et al.*: 2002, *Astrophys. J.* **575**, 1116.
Ciaravella, A., Raymond, J. C., Thompson, B. J., van Ballegooijen, A., Strachan, L., Li, J., *et al.*: 2000, *Astrophys. J.* **529**, 575.
Cliver, E. W., Webb, D. F., and Howard, R. A.: 1999, *Sol. Phys.* **187**, 89.
Crooker, N. U., Gosling, J. T., and Kahler, S. W.: 2002, *J. Geophys. Res. (Space Phys.)* **107**(A2), 3.
Czaykowska, A., de Pontieu, B., Alexander, D., and Rank, G.: 1999, *ApJ* **521**, L75.
Dere, K. P., Brueckner, G. E., Howard, R. A., Koomen, M. J., Korendyke, C. M., Kreplin, R. W., *et al.*: 1997, *Sol. Phys.* **175**, 601.
Dere, K. P., Brueckner, G. E., Howard, R. A., Michels, D. J., and Delaboudiniere, J. P.: 1999, *Astrophys. J.* **516**, 465.
Dobrzycka, D., Cranmer, S. R., Raymond, J. C., Biesecker, D. A., and Gurman, J. B.: 2002, *Astrophys. J.* **565**, 621.
Dobrzycka, D., Raymond, J. C., Biesecker, D. A., Li, J., and Ciaravella, A.: 2003, *Astrophys. J.* **588**, 586.
Doschek, G. A., Cheng, C. C., Oran, E. S., Boris, J. P., and Mariska, J. T.: 1983, *Astrophys. J.* **265**, 1103.
Dulk, G. A., Leblanc, Y., and Bougeret, J.: 1999, *Geophys. Res. Lett.* **26**, 2331.
Forbes, T. G., *et al.*: 2006, *Space Sci. Revs.*, this volume, 10.1007/s11214-006-9019-8.
Forsyth, R. J., *et al.*: 2006, *Space Sci. Revs.*, this volume, 10.1007/s11214-006-9022-0.
Gallagher, P. T., Dennis, B. R., Krucker, S., Schwartz, R. A., and Tolbert, A. K.: 2002, *Sol. Phys.* **210**, 341.
Gergely, T. E., Kundu, M. R., and Hildner, E.: 1983, *Astrophys. J.* **268**, 403.

Gilbert, H. R., Holzer, T. E., Burkepile, J. T., and Hundhausen, A. J.: 2000, *Astrophys. J.* **537**, 503.
Gilbert, H. R., Serex, E. C., Holzer, T. E., MacQueen, R. M., and McIntosh, P. S.: 2001, *Astrophys. J.* **550**, 1093.
Gopalswamy, N., Kaiser, M. L., Lepping, R. P., Kahler, S. W., Ogilvie, K., Berdichevsky, D., *et al.*: 1998, *J. Geophys. Res.* **103**, 307.
Gopalswamy, N., Kaiser, M. L., Thompson, B. J., Burlaga, L. F., Szabo, A., Vourlidas, A., *et al.*: 2000, *Geophys. Res. Lett.* **27**, 1427.
Gopalswamy, N., and Kundu, M. R.: 1992, *ApJ* **390**, L37.
Gopalswamy, N., Shimojo, M., Lu, W., Yashiro, S., Shibasaki, K., and Howard, R. A.: 2003, *Astrophys. J.* **586**, 562.
Gopalswamy, N., Yashiro, S., Kaiser, M. L., Howard, R. A., and Bougeret, J.-L.: 2001, *ApJ* **548**, L91.
Gosling, J. T., Hildner, E., MacQueen, R. M., Munro, R. H., Poland,A. I., and Ross, C. L.: 1976, *Sol. Phys.* **48**, 389.
Haggerty, D. K., and Roelof, E. C.: 2002, *Astrophys. J.* **579**, 841.
Howard, R. A., Sheeley, N. R., Michels, D. J., and Koomen, M. J.: 1985, *J. Geophys. Res.* **90**, 8173.
Howard, R. A., Sheeley, N. R., Michels, D. J., and Koomen, M. J.: 1986, in: *ASSL Vol. 123: The Sun and the Heliosphere in Three Dimensions*. p. 107.
Hudson, H, Bougeret, J.-L., and Burkepile, J.: 2006, *Space Sci. Revs.*, this volume, 10.1007/s11214-006-9009-x.
Hudson, H. S., Khan, J. I., Lemen, J. R., Nitta, N. V., and Uchida, Y.: 2003, *Sol. Phys.* **212**, 121.
Hundhausen, A. J., Burkepile, J. T., and St. Cyr, O. C.: 1994, *J. Geophys. Res.* **99**, 6543.
Illing, R. M. E., and Hundhausen, A. J.: 1983, *J. Geophys. Res.* **88**, 10210.
Innes, D. E., Inhester, B., Srivastava, N., Brekke, P., Harrison, R. A., Matthews, S. A., *et al.*: 1999, *Sol. Phys.* **186**, 337.
Innes, D. E., McKenzie, D. E., and Wang, T.: 2003, *Sol. Phys.* **217**, 247.
Kahler, S. W., Cliver, E. W., and Cane, H. V.: 1989, *Sol. Phys.* **120**, 393.
Kahler, S. W., and Hundhausen, A. J.: 1992, *J. Geophys. Res.* **97**, 1619.
Kahler, S. W., Reames, D. V., and Sheeley, N. R.: 2001, *Astrophys. J.* **562**, 558.
Kaiser, M. L., Reiner, M. J., Gopalswamy, N., Howard, R. A., St. Cyr, O. C., Thompson, B. J., *et al.*: 1998, *Geophys. Res. Lett.* **25**, 2501.
Kane, S. R.: 1981, *Astrophys. J.* **247**, 1113.
Kayser, S. E., Bougeret, J., Fainberg, J., and Stone, R. G.: 1987, *Sol. Phys.* **109**, 107.
Kerdraon, A., Pick, M., Trottet, G., Sawyer, C., Illing, R., Wagner, W., *et al.*: 1983, *ApJ* **265**, L19.
Khan, J. I., and Aurass, H.: 2002, *A&A* **383**, 1018.
Khan, J. I., and Hudson, H. S.: 2000, *Geophys. Res. Lett.* **27**, 1083.
Klassen, A., Aurass, H., Klein, K.-L., Hofmann, A., and Mann, G.: 1999, *A&A* **343**, 287.
Klassen, A., Bothmer, V., Mann, G., Reiner, M. J., Krucker, S., Vourlidas, A., *et al.*: 2002, *A&A* **385**, 1078.
Klassen, A., Pohjolainen, S., and Klein, K.-L.: 2003, *Sol. Phys.* **218**, 197.
Klecker, B., *et al.*: 2006, *Space Sci. Revs.*, this volume, 10.1007/s11214-006-9018-9.
Klein, K., Khan, J. I., Vilmer, N., Delouis, J., and Aurass, H.: 1999, *A&A* **346**, L53.
Klein, K.-L., Krucker, S., and Trottet, G.: 2003a, *Adv. Space Res.* **32**, 2521.
Klein, K.-L., Schwartz, R. A., McTiernan, J. M., Trottet, G., Klassen, A., and Lecacheux, A.: 2003b, *A&A* **409**, 317.
Klein, K.-L., and Trottet, G.: 1994, In: *AIP Conf. Proc. 294: High-Energy Solar Phenomena – a New Era of Spacecraft Measurements*. pp. 187.
Ko, Y., Raymond, J. C., Lin, J., Lawrence, G., Li, J., and Fludra, A.: 2003, *Astrophys. J.* **594**, 1068.
Krall, J., Chen, J., Duffin, R. T., Howard, R. A., and Thompson, B. J.: 2001, *Astrophys. J.* **562**, 1045.
Krucker, S., Larson, D. E., Lin, R. P., and Thompson, B. J.: 1999, *Astrophys. J.* **519**, 864.
Krucker, S., and Lin, R. P.: 2002, *Sol. Phys.* **210**, 229.

Kundu, M. R., and Stone, R. G.: 1984, *Adv. Space Res.* **4**, 261.
Laming, J. M., Raymond, J. C., McLaughlin, B. M., and Blair, W. P.: 1996, *Astrophys. J.* **472**, 267.
Lantos, P., Kerdraon, A., Rapley, G. G., and Bentley, R. D.: 1981, *A&A* **101**, 33.
Lee, L. C., and Wu, B. H.: 2000, *Astrophys. J.* **535**, 1014.
Li, Y., Luhmann, J. G., Mulligan, T., Hoeksema, J. T., Arge, C. N., Plunkett, S. P., *et al.*: 2001, *J. Geophys. Res.* 25103.
Lin, J., and Forbes, T. G.: 2000, *J. Geophys. Res.* **105**, 2375.
Lin, R. P.: 1998, *Space Sci. Rev.* **86**, 61.
Lin, R. P., Evans, L. G., and Fainberg, J.: 1973, *Astrophys.* **14**, 191.
Linker, J. A., and Mikic, Z.: 1995, in: *Solar Wind Conference*. pp. 60.
Linker, J. A., Mikić, Z., Lionello, R., Riley, P., Amari, T., and Odstrcil, D.: 2003, *Phys. Plasmas* **10**, 1971.
Lyons, M. A., and Simnett, G. M.: 2001, *Solar Phys.* **200**, 203.
MacQueen, R. M., and Fisher, R. R.: 1983, *Solar Phys.* **89**, 89.
Maia, D., Pick, M., Vourlidas, A., and Howard, R.: 2000, *ApJ* **528**, L49.
Maia, D., Vourlidas, A., Pick, M., Howard, R., Schwenn, R., and Magalhães, A.: 1999, *J. Geophys. Res.* **104**, 12507.
Maia, D. J. F., and Pick, M.: 2004, *Astrophys. J.* **609**, 1082.
Mancuso, S., and Abbo, L.: 2004, *A&A* **415**, L17.
Mancuso, S., Raymond, J. C., Kohl, J., Ko, Y.-K., Uzzo, M., and Wu, R.: 2002, *A&A* **383**, 267.
Mann, G.: 1995, *Lecture Notes in Physics*. Springer Verlag, Berlin, vol. 444, pp. 183.
Mann, G., and Luehr, H.: 1994, *ApJS* **90**, 577.
Marqué, C., Lantos, P., and Delaboudinière, J. P.: 2002, *A&A* **387**, 317.
Masuda, S., Kosugi, T., Hara, H., Tsuneta, S., and Ogawara, Y.: 1994, *Nature* **371**, 495.
McComas, D. J., Phillips, J. L., Hundhausen, A. J., and Burkepile, J. T.: 1991, *Geophys. Res. Lett.* **18**, 73.
McKenzie, D. E., and Hudson, H. S.: 1999, *ApJ* **519**, L93.
Mikić, Z., and Lee, M. A.: 2006, *Space Sci. Revs.*, this volume, 10.1007/s11214-006-9012-2.
Moon, Y. J., Choe, G. S., Wang, H., Park, Y. D., Gopalswamy, N., Yang, G., *et al.*: 2002, *Astrophys. J.* **581**, 694.
Moreton, G. E.: 1960, *AJ* **65**, 494.
Moses, D., Clette, F., Delaboudiniere, J.-P., Artzner, G. E., Bougnet, M., Brunaud, J., *et al.*: 1997, *Sol. Phys.* **175**, 571.
Narukage, N., Hudson, H. S., Morimoto, T., Akiyama, S., Kitai, R., Kurokawa, H., *et al.*: 2002, *ApJ* **572**, L109.
Nelson, G. J., and Melrose, D. B.: 1985, *Type II bursts*, Solar Radiophysics: Studies of Emission from the Sun at Metre Wavelengths, pp. 333.
Northrop, T. G.: 1966, in: *ASSL Vol. 5: Radiation Trapped in the Earth's Magnetic Field*. p. 26.
Pearson, D. H., Nelson, R., Kojoian, G., and Seal, J.: 1989, *Astrophys. J.* **336**, 1050.
Pick, M.: 1999, in: Bastian, T. S., Gopalswamy, N., and Shibasaki, K. (eds.), *Proceedings of the Nobeyama Symposium, held in Kiyosato, Japan, Oct. 27-30, 1998* NRO Report No. 479, p. 187.
Pick, M., Maia, D., Wang, S. J., Lecacheux, A., and Hawkins, S. E.: 2003, *Adv. Space Res.* **32**, 2527.
Pike, C. D., and Mason, H. E.: 2002, *Sol. Phys.* **206**, 359.
Pohjolainen, S., Maia, D., Pick, M., Vilmer, N., Khan, J. I., Otruba, W., *et al.*: 2001, *Astrophys. J.* **556**, 421.
Priest, E., and Forbes, T. (eds.): 2000, 'Magnetic reconnection: MHD theory and applications'.
Raoult, A., Pick, M., Dennis, B. R., and Kane, S. R.: 1985, *Astrophys. J.* **299**, 1027.
Raulin, J. P., Kundu, M. R., Hudson, H. S., Nitta, N., and Raoult, A.: 1996, *A&A* **306**, 299.
Raymond, J. C., Blair, W. P., and Long, K. S.: 1995, *ApJ* **454**, L31.

Raymond, J. C., Ciaravella, A., Dobrzycka, D., Strachan, L., Ko, Y.-K., Uzzo, M., *et al.*: 2003, *Astrophys. J.* **597**, 1106.
Raymond, J. C., Thompson, B. J., St. Cyr, O. C., Gopalswamy, N., Kahler, S., Kaiser, M., *et al.*: 2000, *Geophys. Res. Lett.* **27**, 1439.
Reames, D. V.: 1999, *Space Sci. Rev.* **90**, 413.
Reiner, M. J., and Kaiser, M. L.: 1999a, *Geophys. Res. Lett.* **26**, 397.
Reiner, M. J., and Kaiser, M. L.: 1999b, *J. Geophys. Res.* **104**, 16979.
Reiner, M. J., Kaiser, M. L., and Bougeret, J.-L.: 2001, *J. Geophys. Res.* **106**, 29989.
Reiner, M. J., Kaiser, M. L., Plunkett, S. P., Prestage, N. P., and Manning, R.: 2000a, *ApJ* **529**, L53.
Reiner, M. J., Karlický, M., Jiřička, K., Aurass, H., Mann, G., and Kaiser, M. L.: 2000b, *Astrophys. J.* **530**, 1049.
Reiner, M. J., Vourlidas, A., Cyr, O. C. S., Burkepile, J. T., Howard, R. A., Kaiser, M. L., *et al.*: 2003, *Astrophys. J.* **590**, 533.
Robinson, R. D., and Stewart, R. T.: 1985, *Sol. Phys.* **97**, 145.
Saito, K., Makita, M., Nishi, K., and Hata, S.: 1970, *Ann Tokyo Astronomical Observatory* **12**, 51.
Schwenn, R., *et al.*: 2006, *Space Sci. Revs.*, this volume, 10.1007/s11214-006-9016-y.
Sheeley, N. R., J., Wang, Y.-M., Hawley, S. H., Brueckner, G. E., Dere, K. P., Howard, R. A., *et al.*: 1997, *Astrophys. J.* **484**, 472.
Sheeley, N. R., Walters, J. H., Wang, Y.-M., and Howard, R. A.: 1999, *J. Geophys. Res.* **104**, 24739.
Sheeley, N. R., and Wang, Y.-M.: 2002, *Astrophys. J.* **579**, 874.
Sheeley, N. R., Warren, H., and Wang, Y.-M.: 2004, *Astrophys. J.* **616**, 1224.
Sheridan, K. V., Jackson, B. V., McLear, D. J., and Dulk, G. A.: 1978, *Proc. Astron. Soc. Aust.* **3**, 249.
Simnett, G. M.: 2004, *A&A* **416**, 759.
Simnett, G. M., Roelof, E. C., and Haggerty, D. K.: 2002, *Astrophys. J.* **579**, 854.
Simnett, G. M., Tappin, S. J., Plunkett, S. P., Bedford, D. K., Eyles, C. J., Cyr, O. C. S., *et al.*: 1997, *Solar Phys.* **175**, 685.
Srivastava, N., Schwenn, R., Inhester, B., Martin, S. F., and Hanaoka,Y.: 2000, *Astrophys. J.* **534**, 468.
Srivastava, N., Schwenn, R., Inhester, B., Stenborg, G., and Podlipnik, B.: 1999, *Space Sci. Rev.* **87**, 303.
St. Cyr, O. C., Burkepile, J. T., Hundhausen, A. J., and Lecinski, A. R.: 1999, *J. Geophys. Res.* **104**, 12493.
St. Cyr, O. C., Plunkett, S. P., Michels, D. J., Paswaters, S. E., Koomen, M. J., Simnett, G. M., *et al.*: 2000, *J. Geophys. Res.* 18169.
Steinolfson, R. S.: 1985, *Wash. DC Am Geophys. Union Geophys. Monogr. Ser.* **35**, 1.
Sterling, A. C., and Hudson, H. S.: 1997, *ApJ* **491**, L55.
Sui, L., and Holman, G. D.: 2003, *ApJ* **596**, L251.
Svestka, Z., Martin, S. F., and Kopp, R. A.: 1980, in: Dryer, M., and Tandberg-Hanssen, E. (eds.), *IAU Symp. 91: Solar and Interplanetary Dynamics*. pp. 217.
Thompson, B. J., Plunkett, S. P., Gurman, J. B., Newmark, J. S., St. Cyr, O. C., and Michels, D. J.: 1998, *Geophys. Res. Lett.* **25**, 2465.
Tokman, M., and Bellan, P. M.: 2002, *Astrophys. J.* **567**, 1202.
Tousey, R.: 1973, in: Rycroft, M. J., and Runcorn, S. K. (eds.), *Space Research XIII, Proceedings of the 15th Plenary Meeting of COSPAR*, Madrid, Spain, 10–24 May 1972, Akademie-Verlag, Berlin, pp. 713.
Trottet, G.: 1986, *Sol. Phys.* **104**, 145.
Tsuneta, S., Hara, H., Shimizu, T., Acton, L. W., Strong, K. T., Hudson, H. S., *et al.*: 1992, *PASJ* **44**, L63.
Uchida, Y.: 1960, *PASJ* **12**, 376.
Uchida, Y.: 1974, *Sol. Phys.* **39**, 431.

Vourlidas, A., Wu, S. T., Wang, A. H., Subramanian, P., and Howard, R. A.: 2003, *Astrophys. J.* **598**, 1392.
Wagner, W. J., and MacQueen, R. M.: 1983, *A&A* **120**, 136.
Wang, Y.-M., and Sheeley, N. R.: 2002, *Astrophys. J.* **575**, 542.
Wang, Y.-M., Sheeley, N. R., Walters, J. H., Brueckner, G. E., Howard, R. A., Michels, D. J., *et al.*: 1998, *ApJ* **498**, L165.
Warmuth, A., Vršnak, B., Magdalenić, J., Hanslmeier, A., and Otruba, W. : 2004, *A&A* **418**, 1101.
Webb, D. F., Burkepile, J., Forbes, T. G., and Riley, P.: 2003, *J. Geophys. Res. (Space Phys.)* 6.
Webb, D. F., and Cliver, E. W.: 1995, *J. Geophys. Res.* **100**, 5853.
Wild, J. P.: 1950, *Aust. J.Phys.* **3**, 541.
Wu, S. T., Guo, W. P., Michels, D. J., and Burlaga, L. F.: 1999, *J. Geophys. Res.* **104**, 14789.
Yashiro, S., Gopalswamy, N., Michalek, G., and Howard, R. A.: 2003, *Adv. Space Res.* **32**, 2631.
Yokoyama, T., Akita, K., Morimoto, T., Inoue, K., and Newmark, J.: 2001, *ApJ* **546**, L69.
Zhang, J., Dere, K. P., Howard, R. A., and Vourlidas, A.: 2004, *ApJ* **604**, 420.